metals

MDPI

Article

Smelting–Aluminothermic Reduction of Hydrogen Pre-Reduced Manganese Ores in a 200 kW DC Arc Furnace

Dursman Mchabe [1,*], Sello Tsebe [1], Madinoge Mampuru [1], Jafar Safarian [2] and Elias Matinde [1]

[1] Mintek, Private Bag X3015, Randburg 2125, Gauteng, South Africa; sello.tsebe@sms-group.com (S.T.); madinogem@mintek.co.za (M.M.); eliasm@mintek.co.za (E.M.)
[2] Department of Materials Science and Engineering, Norwegian University of Science and Technology (NTNU), Alfred Getz Vei 2, 7491 Trondheim, Norway; jafar.safarian@ntnu.no
* Correspondence: dursmanm@mintek.co.za

Abstract

The escalating demand for sustainable metallurgical practices necessitates innovative approaches to manganese production. The smelting–aluminothermic reduction of hydrogen pre-reduced manganese ores in a direct current (DC) arc furnace offers a resilient and sustainable trajectory for optimizing manganese recovery efficiencies while minimizing waste generation under low-carbon operating conditions. This study presents a comparison of smelting–aluminothermic reduction of two Mn ores pre-reduced with hydrogen using two distinct approaches, namely, a packed-bed vertical retort and a plasma rotary furnace. A 200 kW DC arc furnace was used for smelting. The scope of this assessment integrates technical, environmental, and operational metrics of smelting–aluminothermic reduction. For partial process energy estimation, the considered metrics are power stability metrics, specific energy requirement, and load factor/power-on time. The metrics considered for material are reductant efficiency, elemental accountability, elemental recovery, elemental deportment, and slag-to-metal ratio. For process sustainability, refractory and electrode consumption were considered. The environmental indicators considered include CO_2-equivalent emissions per ton of product, dust and particulate emissions, NO_x/SO_x emissions. This research provides critical insights into the viability and environmental advantages of hydrogen pre-reduction coupled with smelting–aluminothermic reduction for cleaner manganese production.

Keywords: smelting–aluminothermic reduction; hydrogen pre-reduced manganese ore; DC arc furnace

Check for updates

Academic Editor: Man Seung Lee

Received: 23 April 2026
Revised: 15 June 2026
Accepted: 24 June 2026
Published: 14 July 2026

Copyright: © 2026 by the authors. Licensee MDPI, Basel, Switzerland. This article is an open access article distributed under the terms and conditions of the Creative Commons Attribution (CC BY) license.

1. Introduction

Manganese is a critical element in the steel industry, primarily used as a deoxidizer, desulfurizer, and alloying agent to enhance steel's strength and abrasion resistance [1,2]. The global demand for Mn alloys is substantial, with millions of tonnes of high-carbon ferromanganese and silicomanganese produced annually [3]. Traditionally, ferromanganese alloys are produced through carbothermic reduction of manganese ores in submerged arc furnaces [4–6]. This conventional method is highly energy-intensive, consuming 2000–3500 kWh per tonne of alloy, and is a significant contributor to greenhouse gas emissions, typically releasing 1–1.4 tonnes of CO_2 per tonne of metal produced due to the reliance on metallurgical coke as both a reductant and energy source [4–7].

The urgent need to align with global climate targets, such as the Paris Agreement's goal of decreasing CO_2 emissions by 45% by 2030 and achieving net-zero by 2050, necessitates the development of innovative and sustainable manganese production processes [6].

Current pyrometallurgical processes face challenges related to high energy consumption, substantial carbon emissions, and the generation of large volumes of by-products like slag [7,8]. These challenges highlight a critical research gap: the need for cleaner, more efficient, and environmentally benign technologies for manganese extraction.

Smelting–aluminothermic reduction presents a promising alternative to carbothermic processes. This method utilizes aluminum as a reducing agent, which is a highly exothermic reaction, potentially reducing external energy input and offering a pathway for valorizing aluminum-containing industrial wastes like Al dross [3]. Furthermore, the integration of hydrogen (H_2) pre-reduction can significantly improve the overall sustainability of the process. Hydrogen pre-reduction has been shown to accelerate the decomposition of carbonates and facilitate the metallization of manganese oxides, offering a low-emission pathway by reducing reliance on carbon-based reductants and lessening atmospheric gaseous carbon dioxide release [2,6,9]. Studies have investigated the effects of various factors, including temperature, gas composition, and ore characteristics, on the H_2 reduction process, noting that H_2 addition can increase the rate of reduction [6].

The use of direct current arc furnaces in metallurgical applications has gained traction due to several advantages over traditional alternating current furnaces, including better power efficiency, reduced electrode consumption, lower noise levels, and improved heat distribution [10]. These characteristics make DC arc furnaces particularly suitable for processes aiming for high energy efficiency and operational stability.

This study aims to provide a comprehensive comparison of the smelting–aluminothermic reduction of hydrogen pre-reduced manganese ores in a 200 kW DC arc furnace. Specifically, we investigate the comparative performance of two different H_2 pre-reduction approaches (packed-bed vertical retort and plasma rotary furnace) in conjunction with smelting–aluminothermic reduction. The assessment integrates a wide array of technical, environmental, and operational metrics, including partial process estimate energy and resource efficiencies, environmental burdens (e.g., GHG intensity, waste generation), eco-efficiency ratios, and operational sustainability indicators. By doing so, this research seeks to demonstrate the potential of this integrated process for achieving resilient, sustainable, and optimized manganese recovery with minimal environmental impact. The findings contribute to the ongoing efforts towards decarbonizing the metallurgical industry and advancing circular economy principles in metal production. This study further seeks to demonstrate the HAlMan process at a higher technology readiness level (TRL 6). For the background and description of the HAlMan process, the reader is referred elsewhere [11,12]. The originality of this study lies in the application-level demonstration of the HAlMan process on a 200 kW DC arc furnace pilot scale, bridging the critical gap between laboratory-scale concepts and industrial-scale implementation for sustainable manganese production. This research provides a comparative investigation of two distinct hydrogen (H_2) pre-reduction approaches, the packed-bed vertical retort and the plasma rotary furnace, integrated with smelting–aluminothermic reduction. Furthermore, the study contributes a multi-dimensional assessment framework that integrates technical performance with environmental and operational indicators, including GHG intensity, waste generation, and eco-efficiency ratios. By evaluating these integrated process routes, this research demonstrates a viable pathway for decarbonizing the metallurgical industry and advancing circular economy principles in metal production.

2. Materials and Methods

2.1. Materials: Origin, Preparation and Characterization

Two manganese ores were used in this study, namely, United Manganese of Kalahari (UMK) ore and Nchwaning ore. UMK ore (United Manganese of Kalahari Ltd., Hotazel, Northern Cape Province, South Africa); N-ore (Assmang Ltd., Cato Ridge, KwaZulu-Natal Province, South Africa). The two ores differ in mineralogy and grades, and are mined by different companies (e.g., UMK ore is mined byUnited Manganese of Kalahari (UMK) (Pty) Ltd., whereas Nchwaning ore (N-ore) is mined by Hotazel Manganese Mines (HMM), Kalahari Basin, Northern Cape Province, South Africa). The Nchwaning ore used in this study was procured through Assmang (Pty) Ltd., Cato Ridge, KwaZulu-Natal Province, South Africa. The UMK ore was supplied by Transalloys (Pty) Ltd., eMalahleni, Mpumalanga Province, South Africa, South Africa.

The as-received lumpy ores were subjected to comminution and granulometric classification into the −20 mm + 6 mm fraction, which conforms to the stringent operational specifications of Mintek's feed system.

Two distinct pre-reduction approaches were deployed for the hydrogen-mediated conditioning of these ore fragments at elevated temperatures (700–900 °C): (i) a vertical retort-packed bed furnace (VRF) (Figure 1) and (ii) a rotary plasma furnace (sample pre-reduced by SINTEF). The respective equipment were designed and fabricated at Mintek and SINTEF Industry, respectively. The vertical retort-packed bed furnace hydrogen pre-reduction of manganese ore was conducted over 31 batches, with an average of 120 kg of raw lumpy ore charged into the furnace for each batch. The furnace was initially pre-heated under an argon atmosphere flowing at 21.5 Sl/min until the charge reached 500 °C. At this threshold, the Ar was gradually displaced by H_2 gas at a constant flow rate of 112.5 Sl/min. Heating continued until the target reduction temperatures were achieved: 750 °C for N-ore and 800 °C for UMK. These operating temperatures were selected based on prior laboratory-scale optimization studies [13,14]. The pre-determined residence times employed in this study are 6, 8, 10, 12, and 16 h. Upon completion of the residence time, the H_2 flow was terminated, and the furnace was allowed to cool under Ar flowing at 21.5 Sl/min to maintain an inert atmosphere and prevent re-oxidation of the reduced ore. Once cooled to ambient temperature, the material was discharged into drums fitted with Ar-purged nozzles and subsequently stored in vertical polyvinyl chloride containers under positive Ar pressure.

The pre-reduction of Nchwaning manganese ore lumps in a plasma rotary furnace at the SINTEF Trondheim Laboratories Smelting Hall was conducted over three campaigns. During pre-reduction, a hydrogen flow rate of 350 Sl/min was used, and the material temperature ranged from 800 to 900 °C. A residence time of 15.07 h was used.

The degree of pre-reduction (R) was directly determined by monitoring the change in oxygen content over time. LECO analysis was conducted using LECO ONH836 (LECO Corporation, St. Joseph, MI, USA) while employing Standard ASTM E1019 [15]. It is noteworthy to mention that the plasma rotary furnace oxygen values were normalized to dry calcine basis on the basis of Mn concentration of 48.66 mass % and the O/Mn ratio of 1.5 [16].

Complementary raw materials incorporated into this study include flux (burnt lime), which was supplied by Idwala Industrial Holdings (Idwala Lime), Vereeniging, Gauteng Province, South Africa, and reductant (metallic aluminum). Commercial recycled aluminium scrap was supplied by Alitrop Ltd., Johannesburg, Gauteng Province, South Africa. Burnt lime was also subjected to crushing and granulometric refinement (−20 mm + 6 mm) to ensure feed-system compatibility, while the aluminum required only screening to the prescribed size interval for operational integration. The images showing the appearance

of pre-reduced Nchwaning ore, pre-reduced UMK ore, burnt lime, and aluminum are presented in Figure 2.

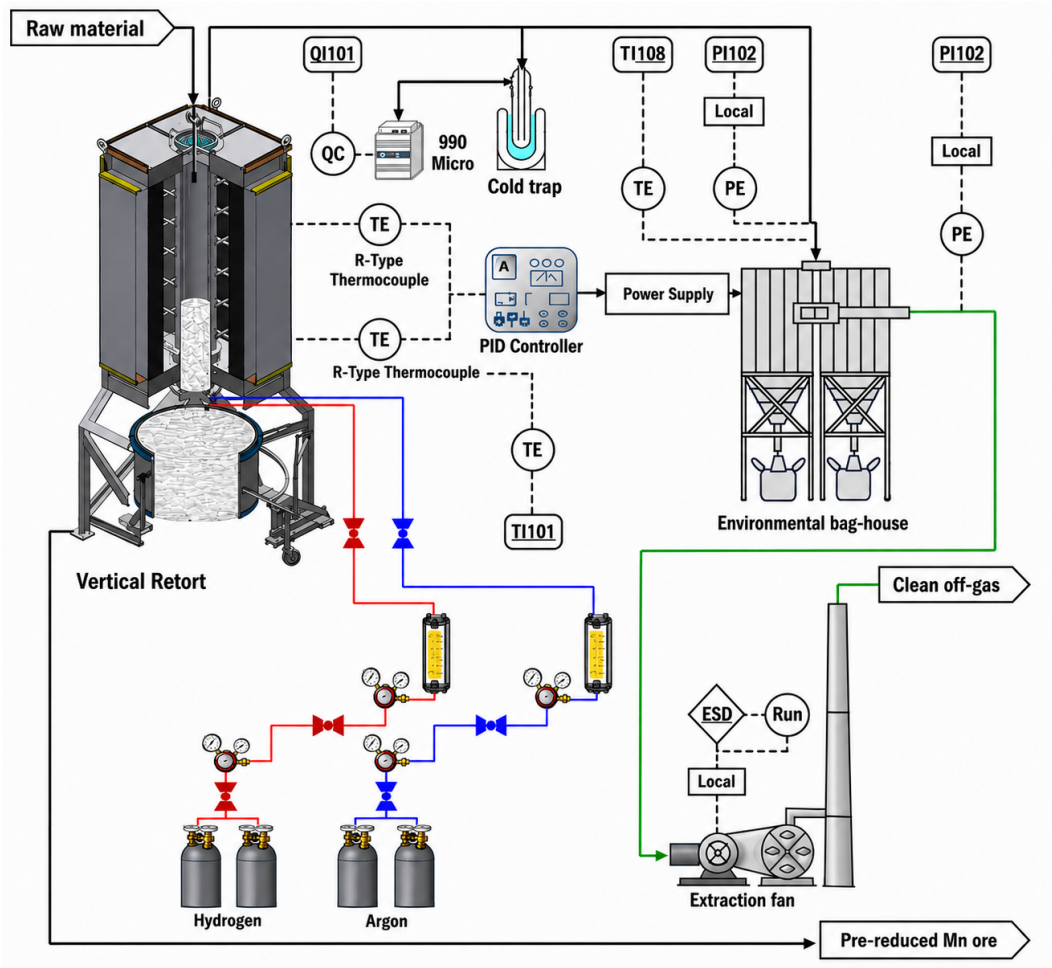


Figure 1. A schematic representation of the vertical retort facility.

2.1.1. Chemical Analyses

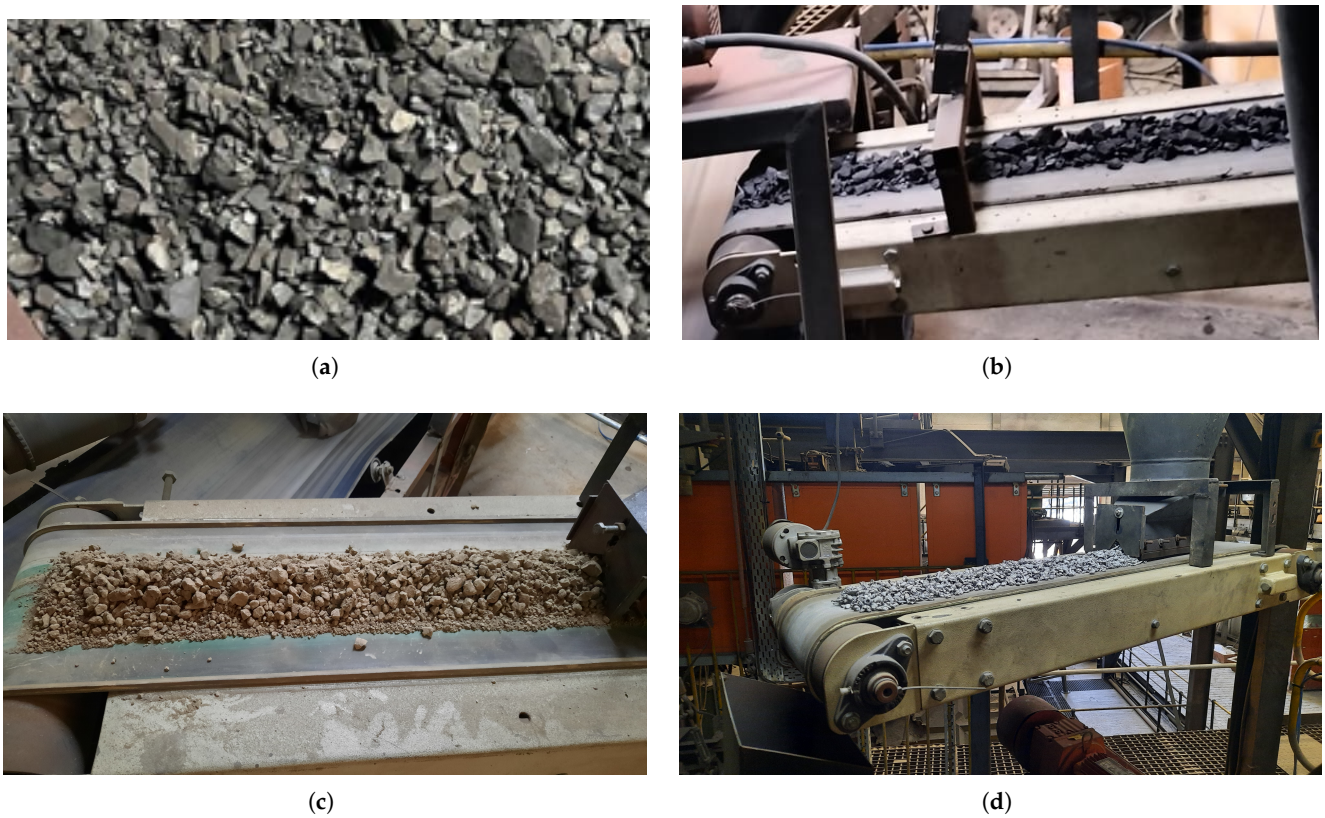
UMK pre-reduced ore, Nchwaning pre-reduced ore (both from Mintek and from SINTEF), and lime were subjected to chemical analyses, which employed Inductively Coupled Plasma–Optical Emission Spectrometry (ICP-OES). The Mintek internal reference material, SARM16, was used. The obtained results are summarized in Tables 1 and 2. Species present at concentrations in the parts-per-million (ppm) range, as well as the loss on ignition, are not reported in Table 1. Thus, the percentages will not add to 100 percent. For mineral-assay reconciliations, the inductive coupled plasma optical emission spectroscopy (ICP-OES) results were used to validate the mineral abundance data obtained from X-ray diffraction (Section 2.1.3).

Table 1. Chemical composition of UMK ore pre-reduced in a VRF, Nchwaning ore pre-reduced in a VRF, Nchwaning ore pre-reduced in a PRK and lime (mass %).

	Al_2O_3	CaO	Fe	MgO	MnO	SiO_2
UMK pre-reduced in VRF	0.33	16.54	6.81	3.70	54.90	5.65
N-Ore pre-reduced in a PRK	0.41	8.17	12.74	1.54	66.78	2.95
N-Ore pre-reduced in a VRF	0.31	7.43	11.11	1.58	62.78	3.70
Lime	0.30	91.93	0.30	<0.005	0.90	1.99

Table 2. X-Ray Fluorescence analyses of recycled scrap aluminum (mass %).

	Al	Si	Cu	Zn	Fe	Mn	Mg
Recycled scrap aluminum	92.50	3.00	1.70	1.40	0.80	0.30	0.30



(**a**) (**b**)

(**c**) (**d**)

Figure 2. Appearance of (**a**) Nchwaning ore, (**b**) UMK ore, (**c**) burnt lime, and (**d**) aluminum on the feed-system's designated conveyor belts.

2.1.2. Analytical Uncertainty

The precision of the calculated indicators is dependent on the uncertainty of the techniques employed. For chemical analyses, the high-precision ICP-OES and LECO combustion methods were utilized to minimize error in elemental recovery calculations. The chemical analytical techniques used in this study are summarized in Table 3, together with the analytes and lower detection limits, and uncertainty. For the average measured gaseous emissions Table 4, the US EPA Methods 1, 2, 3A, 4, 5, 6C, and 7E were followed, and the respective uncertainty values are presented in Section 3.1.4 below.

Table 3. Analytical techniques, analytes, detection limits, and uncertainties.

Analytical Technique	Analytes	Lower Detection Limit	Uncertainty
ICP_BASE_METAL_SLD (ICP-OES)	Al, Ca, Co, Cr, Cu, Fe, Mg, Mn, Ni, Pb, Si, Ti, V, Zn and P_2O_5	0.05%	<2%
Combustion method by LECO	Total C and S	0.01%	<2%
Colorimetry	P or P_2O_5	10 ppm	±5%
XRF_Q_SCAN	All elements with atomic number > 11	Matrix dependent	±2–5%

Table 4. Average measured gaseous emissions from the 200 kW DC arc furnace.

Parameter	Units	Value	Uncertainty
Average Particulate Matter	mg/Nm^3	3.5	±1.14 mg
Average Sulfur Dioxide (SO_2)	mg/Nm^3	0	±18.87 ppm (detection limit)
Average Oxides of Nitrogen (NO_x)	mg/Nm^3	3.49	±6.67 ppm
Average Carbon Dioxide (CO_2)	mg/Nm^3	775	N/A (ambient background)
Average Oxygen (in stack)	$\%v/v$	20.8	±0.22%

The reliability of these analyses is further validated through accountability (mass balance closure) for the main indicators. The study achieved accountability values of 95.40% for Mn, 103.46% for Fe, 97.93% for Al, and 96.34% for Si. These values fall within the industry-standard range of ±10% for high-temperature smelting, confirming that the analytical methodology is suitable for recovery and deportment analysis.

2.1.3. Mineralogical Analyses

For XRD mineralogical analyses, the pre-reduced manganese ore samples were first pulverized and then micronized to achieve a particle size below 20 μm, thereby ensuring more representative data for mineral and elemental quantification. The samples were subjected to the Bruker D8 diffractometer (Bruker Corporation, Billerica, MA, USA) equipped with Fe-filtered Co Kα radiation, and ran over a 2 theta range of 5–80 degrees with a step size of 0.02 degrees 2 theta. Minerals were initially identified using Bruker EVA® software, version 4.2.2, while the quantification of minerals was performed using TOPAS® software, version 4.2. Since pre-reduction was performed batch-wise, the XRD results from successive tests were used to inform the optimization of the operating conditions (e.g., temperature, holding time, gas-to-solid ratio, and so forth) for the next batch.

2.2. Smelting Operations

The 200 DC arc furnace testing facility housed at the Bay 1 area of Mintek was used in this study. A schematic representation of the facility layout is presented in Figure 3, highlighting the major operational domains. For brevity, auxiliary systems (e.g., the cooling-water circuit, gas pipelines, and so forth) are not depicted in the diagram. The facility extends over two floors and consists of three primary operational domains, namely:

- *Feed section*: This domain is endowed with raw material hoppers, conveyor systems, and a mixing bin for charge preparation.
- *Furnace section*: This zone incorporates a hydraulic electrode-control system, a robust furnace shell lined with refractories, and integrated cooling-water circuits.
- *Off-gas handling section*: This section is furnished with an off-gas port, dedicated extraction lines, and a baghouse system for effective dust capture and emissions control.

The feed and furnace sections are equipped with an instrumentation network, enabling real-time, remote monitoring and precise operational control. Conversely, the off-gas realm is not endowed with instrumentation, compelling persistent on-site vigilance and physical inspections to ensure reliability and continuity of operation. Thermal management was ensured through a dedicated cooling-water circuit that continuously cycled water through both furnace and off-gas ducting components. The facility is equipped with gas pipeline infrastructure, ensuring a reliable supply of essential utilities such as compressed air and oxygen.

2.2.1. Experimental Framework

Part of the experimental framework of HAlMan Campaign 1 (Table 5) was systematically configured to investigate four critical process and operational conditions during the smelting of Nchwaning samples pre-reduced via packed-bed vertical retort furnace (Mintek) and rotary plasma furnace (SINTEF), respectively. It is worth noting that the first part of Campaign 1 (Taps 1C1 to 20C1) was dedicated to the smelting–aluminothermic reduction of a different feed material (not part of this study). While these initial taps are not listed in Table 5, which focuses on the core investigation of hydrogen pre-reduced Nchwaning and UMK ores, their contaminating impact affects the elemental accountability data. Residual elements from these Taps 1C1 to 20C1 feed material resulted in the contamination of the metal and slag phases in the early taps of the pre-reduced ore trials. Tap 21 marked the introduction of the new pre-reduced feed material, as detailed in the experimental plan.

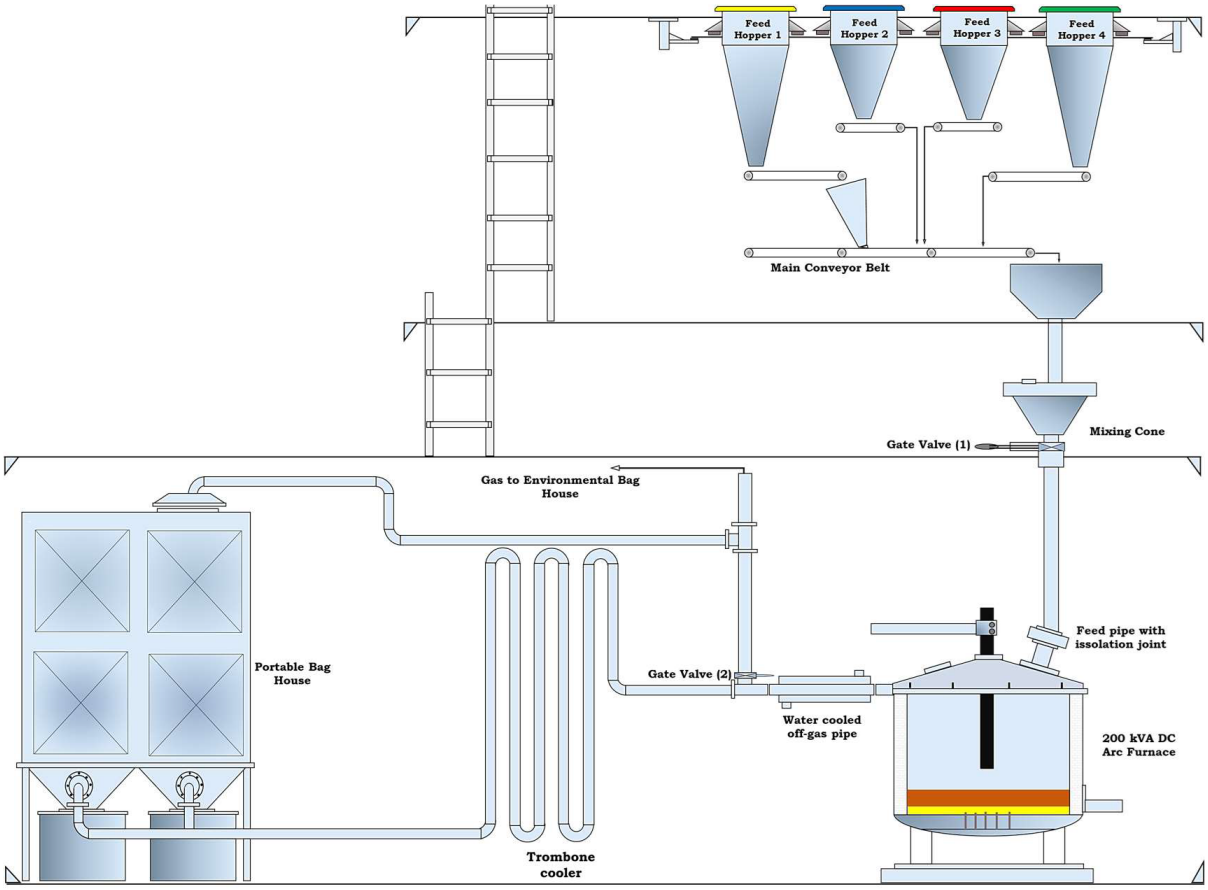


Figure 3. A schematic representation of the Mintek pilot-scale 200 kW DC arc furnace facility layout showing the three sections, namely, feed, furnace and off-gas handling section.

A pivotal transition from Taps 1C1 to 20C1 material to Nchwaning ore pre-reduced using a packed-bed vertical retort furnace induced reduced slag volumes and elevated bath temperatures, necessitating specific energy requirement (SER) modulation (0.95 to 0.85, in taps 24 through 26) to re-anchor the system at 1550 °C. For the Nchwaning ore pre-reduced using the rotary plasma furnace, suppression of MnO in the slag (<4 mass%) was again achieved by increasing the Al addition (from 26.0 to 28.6 kg in Taps 27–29). The final condition (taps 30–36) explored the flux–reductant synergy, wherein lime addition was increased from 26.7 to 30.0 kg, and Al additions were increased from 28.6 to 32.0 kg. Overall, these trials provided information on Nchwaning ore pre-reduced by employing two different approaches, namely, the packed-bed vertical retort furnace and rotary plasma furnace.

The experimental framework of HAlMan Campaign 2 (Table 6) comprises nine conditions designed to investigate the furnace stability, compositional control, ore transitions, and power scaling. Condition 1 (taps 1–5) sought to stabilize the furnace with regard to energy and mass, yet arc instability at 100 V necessitated a reduction to 70 V, alongside increases in SER (0.85 to 0.95). In pursuit of alloy and slag compositions targets, both the reductant (Al) and the flux (lime) were increased, namely, aluminum (9 to 30 kg), and lime (20 to 28 kg). With targets unmet, Condition 2 (taps 6–8) further intensified reagent inputs (Al: 30 to 34 kg; CaO: 28 to 32 kg) and raised SER (0.95 to 1.0). Condition 3 (taps 9–11) explored lime fineness under 90 V, while Condition 4 (taps 12–15) saw the increase in power from 130 kW to 150 kW at 100 V.

Condition 5 (taps 16–18) marked the transition from pre-reduced UMK ore to pre-reduced Nchwaning ore, with slag withheld at tap 16 and voltage reduced to 90 V. Analogous to earlier UMK ore, Condition 6 (taps 19–21) increased SER, Al, and lime modestly (to 1.05, 36 kg, 34 kg, respectively), while Condition 7 (taps 22–24) advanced these inputs further (SER 1.15, Al 40 kg, CaO 38 kg). Condition 8 (taps 25–27) revisited high-power operation (150 kW, 100 V), which was carried forward as Condition 9 (taps 28–30).

Together, these conditions established a systematic progression of operational perturbations, elucidating the coupled roles of voltage, SER, fluxing additions, and ore transition in stabilizing furnace operations and aligning slag–alloy compositions. Campaigns 1 and 2 generated data that integrates technical, environmental, and operational metrics of smelting–aluminothermic reduction. In this study, partial process estimate energy and material balances, quantification of environmental burdens, and indicators of process sustainability are covered.

2.2.2. Sensitivity and Error Sources

A sensitivity analysis was inherently performed by implementing controlled process changes (see column 15 of Table 5). These adjustments tested the system's response to variations in:

- *Feed material*: Transitions between UMK and Nchwaning ores.
- *Energy input*: Systematic adjustments to SER (0.80 to 0.95 kWh/kg) to observe effects on slag temperature and MnO reduction.
- *Reductant addition*: Increasing Al addition from 0.26 to 0.32 to reach specific MnO targets in the slag.

Operational indicators such as power stability were also monitored. Voltage instabilities and voluntary reductions directly influenced the delivered power, contributing to the observed ±5% deviation in mass balance accountability. The other factors that influence the precision of the indicators, including the material heterogeneity, sampling constraints, weighing errors, and so forth, are also considered to be inherent experimental challenges that contribute to the observed ±5% deviation in accountability.

2.2.3. Reliability and Reproducibility

The results for Campaign 2 are derived from a total of 30 individual taps (Taps 1C2 to 30C2), providing a statistically significant dataset for evaluating process stability and reproducibility. The experimental plan for key conditions is detailed in Table 5, where each condition was maintained over multiple taps to ensure the system reached a steady state.

The reliability and reproducibility of the Campaign 2 results are supported by a robust dataset comprising 30 sequential taps (Taps 1C2 to 30C2). To evaluate process stability, the experimental conditions were grouped into discrete intervals where setpoints were held constant to allow the system to reach a steady state, as detailed in Table 7.

Table 5. Mintek Campaign 1 experimental plan.

Condition	Tap No	SER	Power	Heatloss	Feedrate	Tap Time	Pre-Reduced N-Ore		% Al & CaO Addition		Al and CaO Masses, kg		Process and Operational Changes
		(kWh/kg)	(kW)	(kW)	(kg/h)	(h)	Mintek (kg)	SINTEF (kg)	Lime	Al Metal	Lime	Al Metal	
6	21–23	0.95	130	70	63.35	2.41	100	0.00	0.27	0.26	26.70	26.00	New feed material. Transition and stabilization condition.
7	24–26	0.85	130	70	70.84	2.16	0.00	100	0.27	0.26	26.70	26.00	New feed material. Reduced SER due to high slag temperature. Reduced SER due to high slag temperature.
8	27–29	0.85	130	70	92.74	1.67	0.00	100	0.27	0.29	26.70	28.60	Increased Al addition to reach MnO target in slag. Increased SER to increase the slag temperature.
9	30–36	0.80	130	70	75.00	2.16	0.00	100	0.30	0.32	30.00	32.00	Increase lime to 30% and Al to 32%, and the SER to 0.800.

Table 6. Mintek Campaign 2 experimental plan.

Condition	Tap No.	SER	Power	Power Density	Voltage	Heatloss	Feedrate	Time	Pre-Reduced Ore, kg		% Al and CaO Addition		Al and CaO Masses, kg		Process and Operational Changes
		(kWh/kg)	(kW)	(kW/m^2)	(V)	(kW)	(kg/h)	(h)	UMK	N-Ore	Al	Lime	Al	Lime	
Warm-up	0							12.00							
1	1–5	0.80	130	260	70	70	75	2.22	100		0.09	0.20	9	20	Thermal and chemical stabilisation condition. Drop the voltage to 70 V in the next tap. Increased SER, and lime and Al additions.
2	6–8	1.00	130	260	70	70	60	3.27	100		0.34	0.32	34	32	Changed Al and CaO addition as well as SER.
3	9–11	1.00	130	260	70	70	60	3.27	100		0.34	0.32	34	32	Increased voltage to 90 V.
4	12–15	1.00	150	300	100	70	80	2.58	100		0.34	0.32	34	32	Increased power to 150 kW and voltage to 100 V. Tap metal, approx. Half a ladle, stop when there is slag. Drain the furnace to prepare for an ore change.
5	16–18	1.00	130	260	100	70	60	3.27		100	0.34	0.32	34	32	Slag was not tapped in order to rebuild buffer slag in furnace. Chemical stabilisation condition of the new Mn ore. Drop voltage to 90V to lower shell temperatures.
6	19–21	1.05	130	260	90	70	57	3.48		100	0.36	0.34	36	34	Increase Al, lime, and SER.
7	22–24	1.15	130	260	90	70	52	3.91		100	0.40	0.38	40	38	Increase Al, lime, and SER.
8	25–27	1.15	150	300	100	70	70	3.06		100	0.40	0.38	40	38	Increased power, voltage, and SER.
9	28–30	1.15	150	300	100	70	70	3.06		100	0.40	0.38	40	38	Maintain power, voltage, and SER.

Table 7 provides the exact experimental values for mass fed, power, Specific Energy Consumption, current, and voltage for each tap interval. These data were used to calculate the mean values and standard deviations for each operational phase.

The resulting variability is illustrated in Figure 4, where error bars represent the standard deviation of the measured parameters. For example, during the interval 1C2–2C2, the process maintained a mean power of 118.11 ± 5.24 kW and a voltage of 80.45 ± 0.11 V. These error bars provide a quantitative measure of the transient disturbances and arc instabilities inherent in the smelting process, ensuring a transparent representation of data spread across the 30-tap campaign.

Table 7. Summary of process parameters with mean values and standard deviations for each tap interval.

Tap No.	Mass Fed (kg)			Power (kW)			SER (kWh/kg)			Current (A)			Voltage (V)		
	Value	Mean	Std Dev	Value	Mean	Std Dev	Value	Mean	Std Dev	Value	Mean	Std Dev	Value	Mean	Std Dev
1	129	146.40	0.00	110.71	118.11	5.24	0.83	0.97	0.06	1172.98	1412	7.74	89.30	80.45	0.11
2	129			118.12			0.91			1162.04			89.46		
3	158			118.92			1.01			1337.54			82.13		
4	158	158.00	0.00	123.20	120.57	2.30	1.09	1.04	0.04	1734.13	1574	209.30	69.53	74.49	6.71
5	158			119.58			1.02			1651.82			71.81		
6	166			121.10			1.07			1613.90			73.65		
7	166	166.00	0.00	129.25	125.39	4.09	1.07	1.08	0.02	1758.59	1698	75.32	71.66	72.36	1.12
8	166			125.82			1.10			1722.53			71.77		
9	166.6			128.68			1.22			1750.98			72.27		
10	166	166.42	0.36	116.96	121.56	6.26	1.42	1.30	0.10	1505.00	1496	259.84	73.98	79.42	10.94
11	166.66			119.03			1.27			1231.54			92.01		
12	166.11			146.82			1.07			1428.75			100.21		
13	166.18	166.19	0.08	148.33	145.27	2.74	1.13	1.08	0.05	1439.43	1414	24.11	100.24	99.03	1.89
14	166.16			142.85			1.02			1390.71			96.25		
15	166.30			143.07			1.10			1395.63			99.42		
16	166.11			129.16			1.04			1257.57			100.48		
17	166.00	166.05	0.06	125.44	128.24	2.47	1.05	1.04	0.01	1363.25	1345	79.83	89.97	93.85	5.77
18	166.04			130.11			1.03			1414.05			91.09		
19	170.00			128.75			1.09			1384.74			91.19		
20	170.04	170.04	0.05	125.30	127.72	2.11	1.05	1.11	0.07	1362.06	1376	12.22	88.16	91.02	2.77
21	170.09			129.12			1.19			1381.28			93.70		
22	178.14			127.23			1.18			1374.61			91.23		
23	178.04	178.09	0.05	120.00	122.06	4.51	1.18	1.20	0.03	1295.35	1331	40.24	85.66	88.68	2.81
24	178.09			118.95			1.23			1322.88			89.14		
25	178.01			138.67			1.16			1367.23			93.95		
26	178.18	178.09	0.09	146.14	142.75	3.78	1.15	1.14	0.02	1448.71	1416	43.16	98.27	96.18	2.16
27	178.08			143.44			1.12			1432.66			96.33		
28	178.14			133.23			1.15			1341.11			91.87		
29	178.13	178.14	0.01	143.06	139.48	5.43	1.30	1.28	0.12	1453.58	1390	57.70	97.20	96.18	3.90
30	178.15			142.14			1.38			1374.95			99.46		

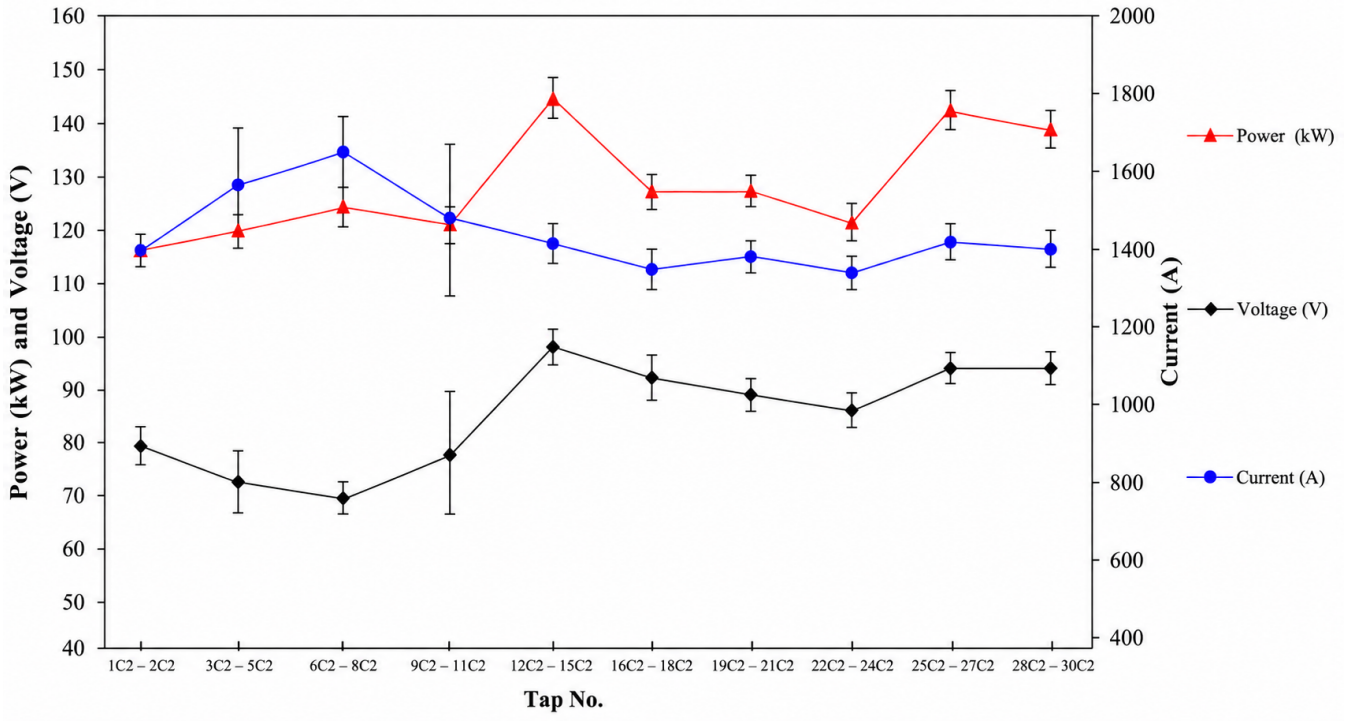


Figure 4. Error bars for power, voltage, and current measurements.

3. Results

3.1. Effect of Pre-Reduced Ores Properties

3.1.1. Extent of Pre-Reduction

The results of the reduction of manganese ores from the vertical retort furnace and the plasma rotary kiln furnace are presented in Tables 8 and 9 below. The reduction of the manganese ore in the vertical retort furnace was calculated using two approaches, namely, fractional removal of oxygen and the gravimetric approach. For the reduction of manganese in the plasma rotary furnace, only the latter approach was used. The first approach follows Equation (1) and is a standard metric in metallurgical kinetics and has been extensively applied in studies of both iron ore [17,18] and manganese ore pre-reduction [2,19].

$$R_{Ext}(\%) = \left(\frac{O_0 - O_t}{O_{Tot}}\right) \times 100 \quad (1)$$

where O_0, O_t and O_{Tot} denote the oxygen content at the initial state, at time t and total removable oxygen respectively. For brevity, the evaluation of O_{Tot} from QXRD results is provided as Supplementary Information. The later approach follows Equation (2)

$$R_{Deg}(\%) = \left(\frac{W_0 - W_t}{W_0 \times f}\right) \times 100 \quad (2)$$

where W_0 is the initial sample weight, W_t is the weight at time t, and f represents the theoretical weight loss fraction (0.22 for UMK and 0.15 for Nchwaning ores [6,13]).

The selection of temperatures for the pre-reduction of Nchwaning and UMK ores was informed by the kinetics studies of Refs. [13,14]. Specifically, Sarkar et al. [13] reported that temperatures between 700 and 800 °C are optimal for Nchwaning ore to ensure rapid reduction while avoiding excessive sintering.

Table 8. Pre-reduction of UMK and Nchwaning ores at different residence times. O_0 is the initial oxygen content, O_t is the oxygen content at the end of the residence time t, and O_{Tot} is the stoichiometric maximum removable oxygen determined from the QXRD mineralogical composition (Supplementary Information). R_{Ext} is the fraction of O_{Tot} removed (Equation (1)). R_{Deg} is the gravimetric extent of reduction using the theoretical mass-loss fraction f ($f = 0.22$ for UMK and $f = 0.15$ for Nchwaning; Equation (2)).

Ore	t (h)	O_0 (%)	O_t (%)	O_{Tot} (%)	R_{Ext} (%)	W_0 (kg)	W_t (kg)	R_{Deg} (%)
UMK	0	27.30	27.30	18.00	0.00	120	120	0.00
UMK	10	27.30	15.45	18.00	65.83	120	99	76.79
UMK	12	27.30	15.13	18.00	67.61	120	103	61.11
Nchwaning	0	21.20	21.20	17.00	0.00	120	120	0.00
Nchwaning	10	21.20	18.48	17.00	16.00	120	107	68.14
Nchwaning	16	21.20	15.33	17.00	34.53	120	108	64.77

As shown in Table 8, UMK ore achieved a significantly greater extent of reduction (65.83%) and reduction degree (76.79%) compared to Nchwaning ore (16.53% R_{ext} and 68.14% R_{deg}) under residence time of 10 h. This suggests UMK possesses higher reducibility despite its higher initial oxygen content.

The plasma rotary furnace results (Table 9) at 900 °C exhibited fluctuations in reduction levels over time. While a peak R_{ext} of 42.88% occurred at 10 h, subsequent samples showed lower values, potentially due to non-uniform reduction or cooling effects within the rotary environment.

Table 9. Pre-reduction of Nchwaning manganese ore in a plasma rotary furnace at the SINTEF Smelting Hall, Trondheim, Norway. O_0 is the initial oxygen content, O_t is the oxygen content measured at the end of the residence time t (both normalised to a dry calcine basis on the basis of an Mn concentration of 48.66 mass % and an O/Mn ratio of 1.5 [16]), and $O_{Tot} = 17.00\%$ is the stoichiometric maximum removable oxygen deduced from QXRD results (provided as Supplementary Information). R_{Ext} is calculated according to Equation (1).

Ore	t (h)	O_0* (Mass %)	O_t* (Mass %)	O_{Tot} (Mass %)	R_{Ext} (%)
Nchwaning	0	21.20	21.20	17.00	0.00
Nchwaning	5	21.20	16.81	17.00	25.82
Nchwaning	6	21.20	15.39	17.00	34.18
Nchwaning	9	21.20	16.65	17.00	26.76
Nchwaning	10	21.20	13.91	17.00	42.88
Nchwaning	12	21.20	15.73	17.00	32.18
Nchwaning	14	21.20	15.04	17.00	36.24
Nchwaning	15	21.20	15.25	17.00	35.00

* Normalised to a dry calcine basis on the basis of an Mn concentration of 48.66 mass % and an O/Mn ratio of 1.5 [16].

A. Power Stability Metrics: Arc stability, voltage/current fluctuations

The stability of the electric arc, along with the degree of voltage and current fluctuations, is a critical operational indicator in electric arc furnaces. These metrics directly influence energy efficiency, electrode and refractory life, and overall process performance [20,21].

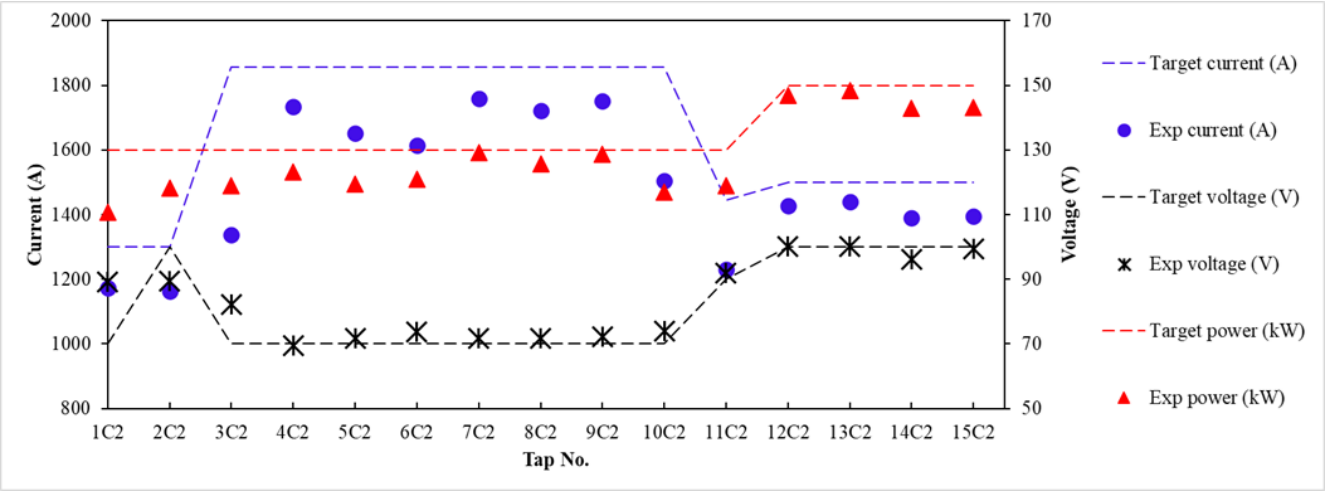
Figure 5 shows the comparison of the set-points (current, voltage, and power) against experimental observed values for the (a) UMK ore pre-reduced in a packed-bed retort furnace, and (b) Nchwaning ore pre-reduced in a packed-bed retort furnace. The voltage instabilities and voluntary voltage reduction directly affect the power stability and reduce delivered power. In many EAF operations, control systems aim to minimize variations in arc voltage and current to maximize power input and stabilize the process [22].

B. Specific energy requirement

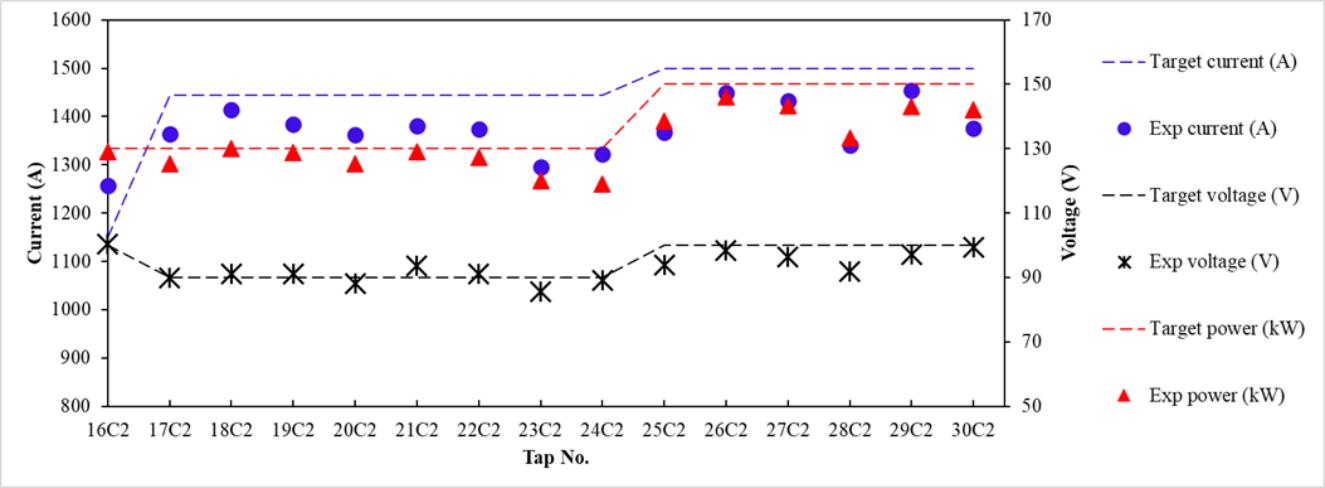
The specific energy requirement (in kWh/kg), is a critical performance indicator in metallurgical processes. In this study, Equation (3) was employed to calculate the specific energy requirement, SER, where the obtained results are plotted in Figure 6.

$$\text{SER} = \frac{\text{Total Energy In} - \text{Total Energy Out}}{\text{Total Feed In}} \quad (3)$$

where Total Energy In refers to the sum of the electrical energy supplied to the DC arc furnace and the chemical energy from the reactions. The Total Energy Out refers to the total enthalpy of the furnace products (slag, alloy, and off-gas) and heat losses at the tapping temperature. It is worth noting that the SER (defined as the electrical energy supplied to the DC arc furnace per kilogram of total feed material) calculation is restricted to the furnace operation stage and does not include the energy for upstream hydrogen production or pre-reduction. However, the mass and energy balances for the pre-reduction of Nchwaning manganese ore based on the ore characteristics and suitable reduction conditions were calculated previously [23]. It was indicated that to calcine and pre-reduce the raw ore in a pre-reduction reactor, about 293.7 Nm^3 H_2 gas per 1 ton pre-reduced ore is used, which corresponds to about 450.5 Nm^3/t FeMn metal product for the optimized condition as the last tapings of the Campaign 2. Assuming the energy consumption of 39.4 kWh/kg H_2 via a state-of-the-art technology for green hydrogen gas production [24], approximately 792.5 kWh/t FeMn is dedicated to the hydrogen production.



(**a**) Retort-packed bed furnace UMK-Ore Power Stability Metrics



(**b**) Retort-packed bed furnace N-Ore Power Stability Metrics

Figure 5. Power stability metrics during smelting of pre-reduced manganese ores: (**a**) UMK ore pre-reduced in a packed-bed retort furnace; (**b**) Nchwaning ore pre-reduced in a packed-bed retort furnace.

While the aluminothermic reaction is exothermic, supplemental electrical energy (represented by the SER) was required to maintain the process temperature at 1550 °C due to the specific thermal balance of the pre-reduced feed. Changes in the target SER setpoint, for instance, an increase from 0.85 to 0.95, then to 1.05 and 1.15 (Conditions 1, 6, and 7, respectively), guide adjustments to other operational parameters, such as aluminum and lime additions and the feed rate, all aimed at achieving the desired energy input per unit of processed material [25]. Increasing Al and lime additions (e.g., in Conditions 1, 2, 6, and 7) affects the chemical energy balance of the furnace.

The specific energy requirement of the smelting process can also be estimated from the slope of a plot of average power against average feed rate (Figure 7), independently of heat losses. The y-intercept of this plot provides an estimation of the heat losses.

Theoretically, mass and energy balance calculations performed using HSC Chemistry yielded energy consumption of 792.5 and 647.9 kWh/t FeMn for the production of dedicated green hydrogen for the reduction of Nchwaning and UMK ores, respectively. However, the theoretical energy consumptions for the smelting and aluminothermic reduction step are significantly lower and approximately 54.6 kWh/t FeMn and 84.1 kWh/t FeMn for Nchwaning and UMK pre-reduced ores, respectively. Hence, the overall energy

consumption is low for the integrated process. However, in the smelting–aluminothermic reduction in pilot scale in this study, the energy consumption (880 kWh/t FeMn) is not close to the low theoretical values due to the heat losses from the furnace body (not considered in theoretical calculations) and also the fact that the charged ore was not fully reduced, and the reductant efficiency was not high enough, as mentioned above. Therefore, under optimum process conditions, the energy consumption can be significantly lower for the smelting–aluminothermic reduction in a future commercial process, indicating a more sustainable process in comparison with SAF technology that has direct energy consumption of about 2000–3000 kWh/t FeMn [12]. It is worth noting that in the HAlMan process, Al reductant is scrap or dross, and hence they have insignificant energy consumption to produce, as they are secondary sources of reductant.

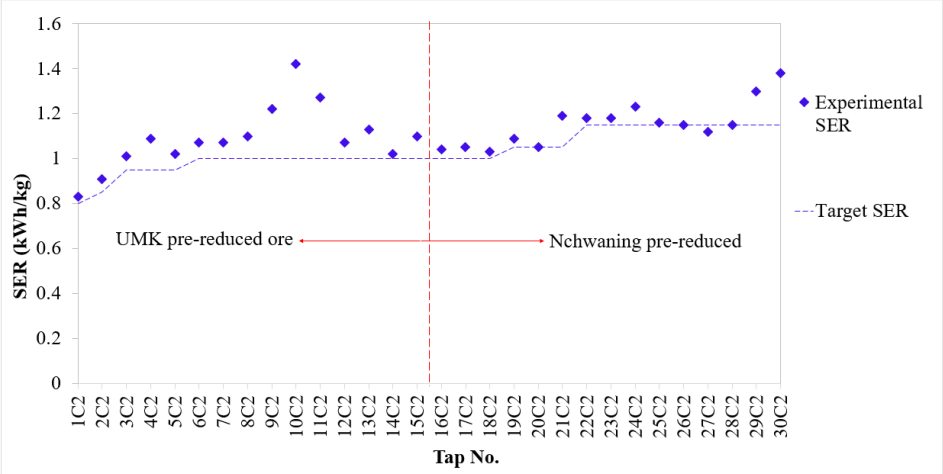


Figure 6. Specific energy requirement during smelting of UMK pre-reduced ore compared with that during smelting of Nchwaning pre-reduced ore.

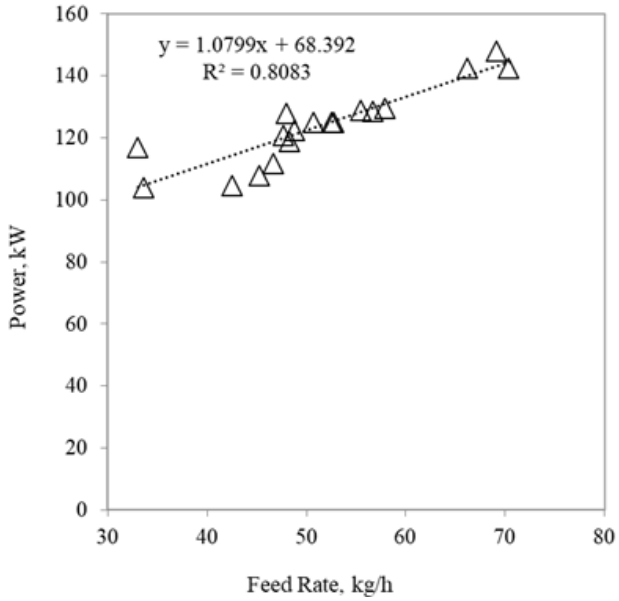


Figure 7. Plot of average furnace power against average feed rate.

C. Load factor/power-on time

The operational efficiency of a smelting process is critically influenced by its load factor (η_{LF}), which represents the proportion of effective smelting time (t_{smelt}) relative to the total operational cycle, including downtime (t_{down}). A high load factor signifies optimized furnace utilization, crucial for economic viability and increased productivity in industrial

applications. This section details the calculated load factors for the three experimental campaigns, providing insight into the operational performance of the respective pre-reduction routes and smelting.

The t_{smelt} is defined as the sum of all tap durations, and t_{down} is the sum of all downtimes, calculated using the following formulas:

$$t_{smelt} = \sum \text{Tap duration} \quad (4)$$

$$t_{down} = \sum \text{Down-time} \quad (5)$$

$$\eta_{LF} = \frac{t_{smelt}}{t_{smelt} + t_{down}} \times 100 \quad (6)$$

The calculated operational metrics for each pre-reduced manganese ore are summarized in Table 10.

Table 10. Summary of calculated load factors for experimental campaigns.

Ore Type	t_{smelt} (h)	t_{down} (h)	η_{LF} (%)
UMK retort-packed bed furnace	48.50	2.08	95.89
Nchwaning retort-packed bed furnace	50.55	1.62	96.89

3.1.2. Alloy and Slag Characterization, Reductant Efficiency and Elemental Mass Balance

A. Metal and slag composition

The chemical compositions of the produced metallic alloy and the corresponding slag phase were analyzed to evaluate the efficiency of the smelting process and the extent of manganese recovery. The results for representative samples, including the final digout, are summarized in Tables 11 and 12.

The metallic phase was primarily composed of manganese and iron, with minor concentrations of silicon. As shown in Table 11, the manganese content in the alloy ranged from 61.90 wt.% to 77.33 wt.%. Notably, the carbon content remained consistently low, ranging between 0.15 wt.% and 0.66 wt.%. This low carbon concentration is characteristic of a refined ferromanganese product rather than standard high-carbon ferromanganese, which typically contains 7–8% carbon [26].

The iron content varied between 17.90 wt.% and 40.01 wt.%, inversely correlating with the manganese concentration. The final digout sample yielded a manganese content of 67.69% and an iron content of 23.06%. These values align with the pilot-scale observations of Mukono et al. [27], who noted that Nchwaning and UMK ore blends typically produce alloys with manganese levels exceeding 65% depending on the reduction conditions.

Table 11. Chemical composition of the metallic phase (mass %) for selected samples.

Sample	Mn	Fe	Si	C	Al	Mg	Ca	Cr	P	S	Cu	Ni	Ti	V	Zn	Pb
1C2	65.25	35.75	0.45	0.59	0.12	0.12	0.05	0.71	0.08	0.01	0.37	0.22	0.05	0.05	0.05	0.22
5C2	77.26	26.40	0.82	0.31	0.05	0.05	0.05	0.55	0.09	0.01	0.96	0.36	0.05	0.05	0.05	0.17
11C2	77.21	21.00	2.98	0.52	0.31	0.05	0.05	0.49	0.10	0.01	1.06	0.33	0.05	0.05	0.05	0.15
15C2	76.80	18.40	3.83	0.22	0.10	0.05	0.05	0.53	0.07	0.01	1.16	0.27	0.05	0.05	0.05	0.14
18C2	73.05	24.60	2.90	0.16	1.01	0.05	0.05	0.35	0.08	0.01	0.99	0.17	0.05	0.05	0.05	0.16
21C2	71.75	25.10	3.27	0.16	2.29	0.05	0.05	0.25	0.09	0.01	1.06	0.10	0.05	0.05	0.05	0.17
24C2	72.15	24.60	3.66	0.20	4.19	0.05	0.05	0.20	0.08	0.01	1.15	0.06	0.05	0.05	0.05	0.17
27C2	65.55	23.40	3.91	0.22	4.70	0.05	0.25	0.18	0.09	0.01	1.32	0.05	0.05	0.05	0.05	0.12
30C2	66.20	19.30	5.31	0.15	7.49	0.05	0.32	0.15	0.08	0.01	0.66	0.05	0.05	0.05	0.05	0.11

The slag composition provides critical insight into the partitioning of manganese between the metal and oxide phases. As indicated in Table 12, the initial MnO concentration in Sample 1C2 was 58.9%, which significantly decreased to 12.45% by Sample 30C2. This depletion of MnO in the slag confirms the high degree of manganese reduction into the metallic phase [28].

A distinctive feature of the slag is the high concentration of Al_2O_3 (up to 52.45%) and CaO (up to 37.5%). The accumulation of these oxides results from the consumption of MnO and SiO_2 during the reduction process and the presence of gangue minerals in the UMK and Nchwaning ores [27]. According to Tangstad et al. [29], the high Al_2O_3 and CaO content significantly influences the slag's liquidus temperature and viscosity, which are paramount for efficient metal–slag separation in the production of manganese ferroalloys.

Table 12. Chemical composition of the slag phase (mass %) for selected samples.

Sample	MgO	Al_2O_3	SiO_2	CaO	Cr_2O_3	MnO	FeO
1C2	7.42	10.55	11.40	16.12	0.22	58.90	9.45
5C2	9.46	38.40	5.56	25.55	0.08	16.70	0.41
11C2	7.55	45.45	1.83	31.85	0.07	11.80	0.94
15C2	7.35	48.45	1.82	37.50	0.07	6.40	0.29
18C2	4.11	48.80	4.18	28.15	0.07	15.80	0.23
21C2	5.27	44.55	3.66	28.15	0.07	18.60	0.32
24C2	4.36	48.10	2.54	29.36	0.07	16.50	0.35
27C2	5.40	49.45	2.18	29.68	0.07	16.05	0.33
30C2	6.33	52.45	1.63	28.45	0.07	12.45	0.26

B. Reductant efficiency

The efficiency of aluminum as a reductant is a pivotal metric in pyrometallurgical operations, particularly when leveraging secondary aluminum sources. It quantifies the effectiveness with which supplied aluminum is consumed for the intended reduction of target metal oxides, specifically manganese, iron, and silicon. Achieving high reductant efficiency is paramount for both economic viability and minimizing the environmental footprint of such processes [3,30]. As defined in Equation (7), η_{Al} represents the ratio of aluminum consumed to produce Mn, Fe, and Si to the total aluminum fed into the furnace.

$$\eta_{Al} = \frac{\text{Al consumed to produce Mn + Al consumed to produce Si}}{\text{Total Al consumed}} \times 100 \quad (7)$$

The reductant efficiencies observed in this study, as shown in Figure 8, demonstrate variability depending on the properties of the respective pre-reduced ores. Nchwaning manganese ore pre-reduced in a retort-packed bed furnace exhibited efficiencies between 30.89% and 55.32%. This can be attributed to the pre-reduction extent of the respective ores via respective pre-reduction approaches, whereas for UMK manganese ore, also pre-reduced in a retort-packed bed furnace, the efficiencies spanned from 19.46% to 56.67%.

C. Elemental accountability

The overall mass accountability provides a measure of the closure of the elemental balance across the smelting system. It compares the total elemental input (from feeds such as aluminum, lime, and pre-reduced ores) with the total output (in metal, slag, and dust streams).

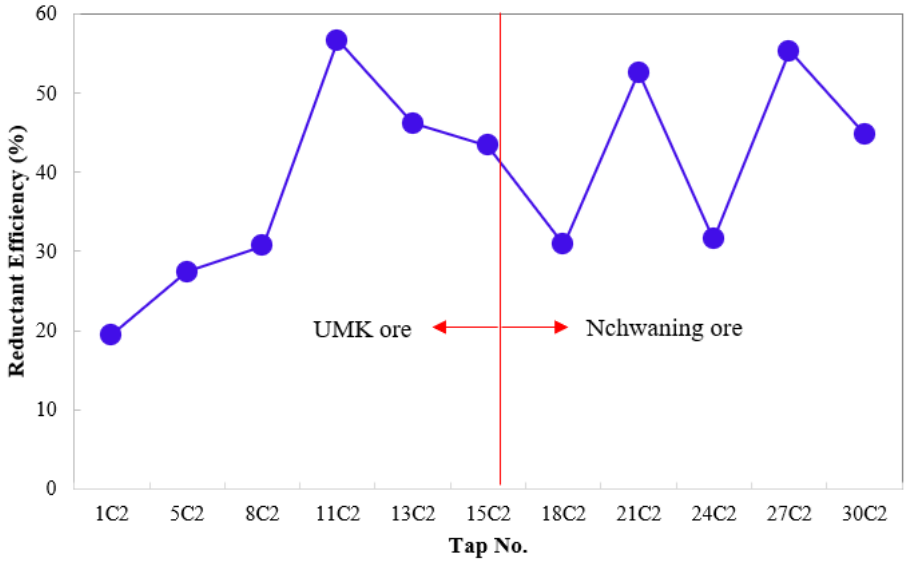


Figure 8. Reductant efficiencies during smelting of pre-reduced manganese ores in a packed-bed vertical retort furnace.

In this study, the accountability of each element was determined to evaluate the degree of mass balance closure within the reduction process. It is defined as the ratio of the total mass of each element exiting the system through all product and by-product streams to the total mass entering the system through feed materials, as given in Equation (8).

$$\text{Accountability}(\%) = \left(\frac{\sum m_{i,\text{out}}}{\sum m_{i,\text{in}}}\right) \times 100 \quad (8)$$

where $m_{i,\text{out}}$ is the mass of element i in all output streams (metal, slag, and dust), and $m_{i,\text{in}}$ is the corresponding mass of element i in all input materials.

Figure 9 presents the overall calculated elemental accountabilities for Al, Ca, Fe, Mg, Mn, and Si for Campaign 2 (Taps 1C2 to 30C2). The overall accountability values ranged from approximately 95.40% for Mn to 103.46% for Fe. Specifically, Al accountability was 97.93%, Fe was 103.46%, Mn was 95.40%, and Si was 96.34%. These values generally exceed 95%, indicating a satisfactory overall mass balance.

D. Elemental recovery

Elemental recovery quantifies the extent to which target species were transferred from the feed materials into the metallic phase. It is a key indicator of the process efficiency and reflects both thermodynamic and kinetic factors governing reduction, phase separation, and alloy formation. The recovery of each element was calculated using Equation (9).

$$\text{Recovery}(\%) = \left(\frac{m_{i,\text{metal}}}{\sum m_{i,\text{in}}}\right) \times 100 \quad (9)$$

where $m_{i,\text{metal}}$ is the mass of element i recovered in the metallic product, and $\sum m_{i,\text{in}}$ is the total mass of that element charged to the system via all input materials.

The overall elemental recovery values into the metal phase are shown in Figure 10. In the metal stream, Fe exhibited a high recovery of 96.44%, and Mn recovery was 65.92%. Si recovery was 42.28%, while Al showed a minor recovery of 3.87%. The elements that were recovered in the slag stream are Al: 94.02%, Fe: 6.61%, Mn: 29.20%, Si: 53.85%, whereas those in the dust stream are Al: 0.04%, Fe: 0.40%, Mn: 0.28%, Si: 0.21%.

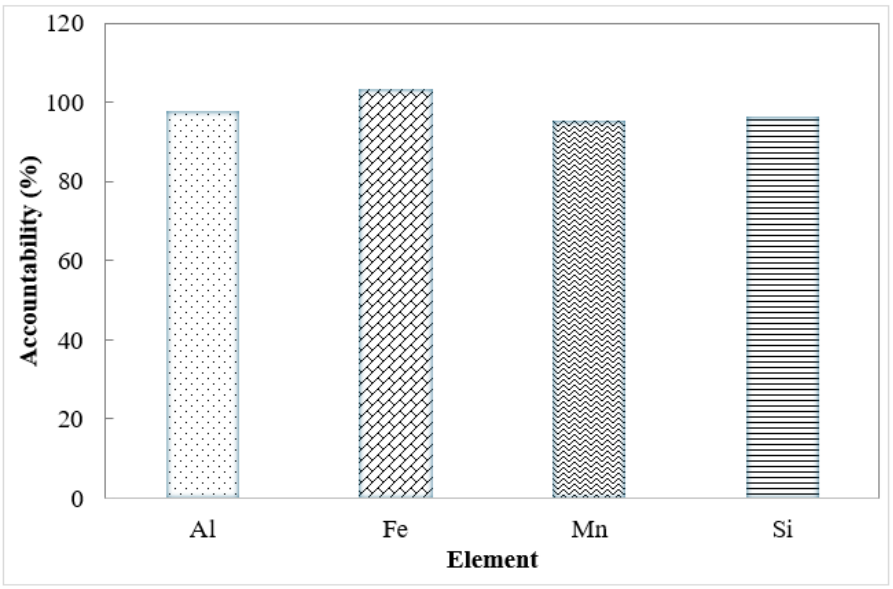


Figure 9. Overall accountability of elements during Campaign 2 (Taps 1C2 to 30C2).

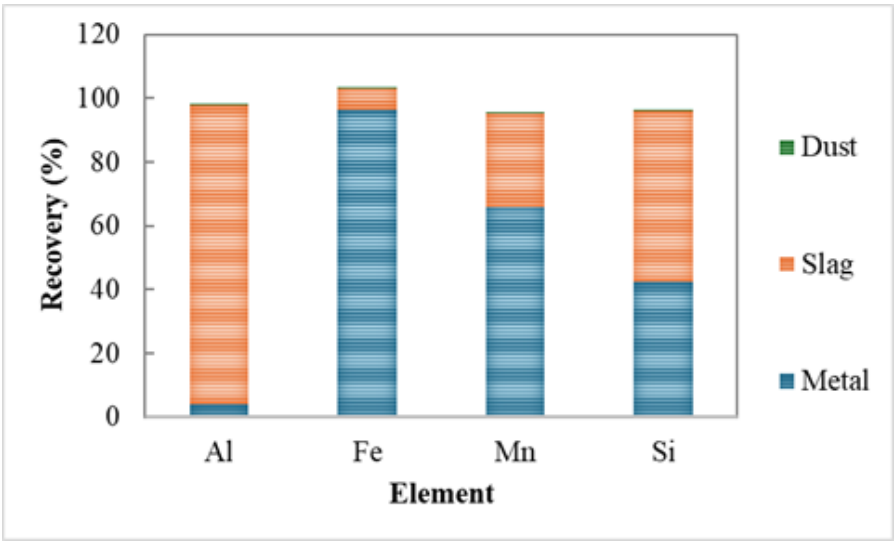


Figure 10. Overall recovery of elements during Campaign 2 (Taps 1C2 to 30C2).

E. Elemental deportment

Deportment describes the distribution of each element among the various product phases, viz:metal, slag, and dust, and provides insight into the selectivity and completeness of reduction reactions. It complements the recovery analysis by indicating how effectively elements were partitioned into their thermodynamically preferred phases [31,32]. The elemental deportment (%) to each phase was determined using Equation (10).

$$\text{Deportment } i,j\left(\frac{mi,j}{\sum m_{i,\text{out}}}\right)\times 100 \quad (10)$$

where $m_{i,j}$ is the mass of element i in phase j (metal, slag, or dust), and $\sum m_{i,\text{out}}$ is the total mass of that element in all output streams.

Figure 11 illustrates the elemental deportment behavior across the process. Fe and Mn predominantly reported to the metallic phase, with 93.22% of Fe and 69.09% of Mn deporting to metal. Si showed a significant deportment to metal at 43.88%. Al, however, was primarily concentrated in the slag (96.01%). Minor amounts of elements were found in the dust stream.

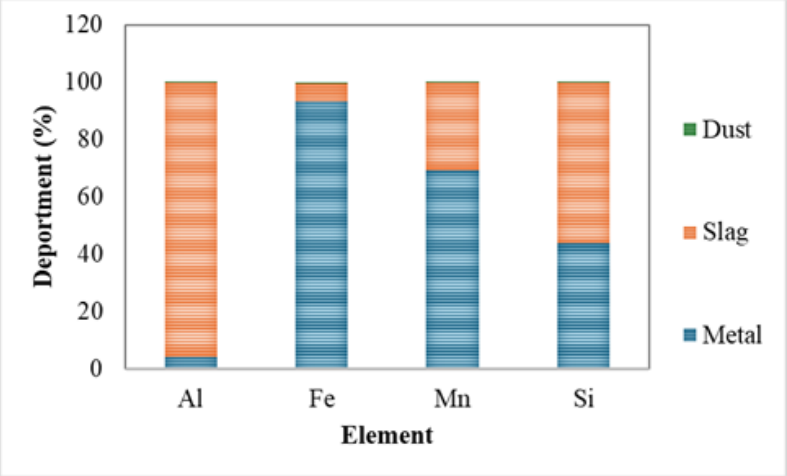


Figure 11. Overall deportment of elements during Campaign 2 (Taps 1C2 to 30C2).

F. Slag-to-metal ratio

The slag-to-metal ratio (SMR), defined as the mass of slag produced per unit mass of metal tapped (kg slag/kg metal), is a key metric for assessing material efficiency, energy demand, and downstream waste management in ferroalloy production. A lower SMR generally indicates more efficient utilization of raw materials and energy, reduced slag handling requirements, and a lower environmental burden. The experimental slag and metal masses obtained in this study are summarized, and the calculated overall SMRs for each campaign are presented in Table 13, derived from the aggregated mass of slag and metal from all taps where both products were successfully obtained, providing a more representative average for each campaign. The overall SMRs ranged from 1.34 kg/kg to 1.87 kg/kg. The individual tap-wise SMRs are also depicted in Figure 12.

Table 13. Overall slag-to-metal ratios during smelting of pre-reduced UMK and Nchwaning ores.

Ore	Total Slag (kg)	Total Metal (kg)	Overall Slag-to-Metal Ratio (kg/kg)
UMK	1015	543	1.87
Nchwaning	944.33	704	1.34

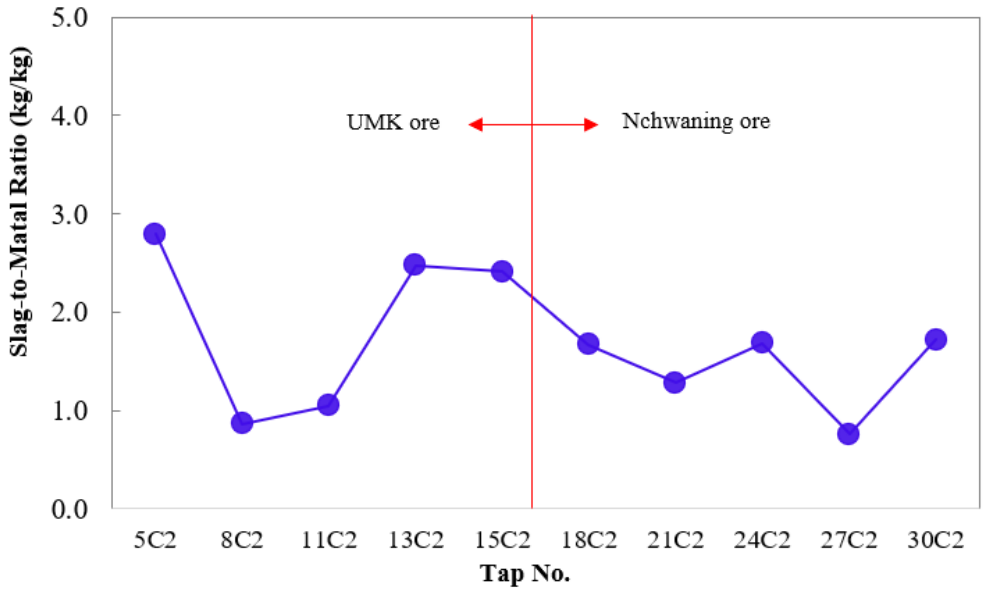


Figure 12. Slag-to-metal ratios during smelting of pre-reduced Mn ores in a packed-bed retort furnace.

3.1.3. Comparative Operations Sustainability Assessment for UMK and Nchwaning Pre-Reduced Ores: Refractory and Electrode Consumption

A. Refractory consumption

Refractory lining degradation is a critical operational and economic factor in high-temperature metallurgical processes, including ferroalloy production. The wear rate of refractory materials directly influences furnace longevity, maintenance schedules, smelting energy efficiency, and overall production costs [33]. In electric arc furnaces, refractory consumption is primarily driven by thermomechanical stress, chemical corrosion by molten slag and metal, and erosion [34]. This section quantifies the refractory consumption during the experimental campaigns and discusses its implications.

Refractory consumption, specifically the loss of magnesia from the furnace lining, was estimated by calculating the difference between the cumulative MgO leaving the system in the slag and the cumulative MgO introduced with the feed materials over each campaign. The results, expressed as kilograms of MgO consumed per kilogram of metal produced, are summarized in Table 14 and in Figure 13.

Table 14. Refractory consumption rates during smelting of pre-reduced Nchwaning and UMK ores.

Ore	MgO Consumed (kg)	Metal Produced (kg)	Refractory Consumption Rate (kg MgO/kg Metal)
UMK retort-packed bed furnace	99.28	543	0.1828
Nchwaning retort-packed bed furnace	74.03	704	0.1051

The refractory consumption rates varied between 0.1051 kg MgO/kg metal and 0.1828 kg MgO/kg metal across the two pre-reduced ores. Refractory consumption rates are highly dependent on specific furnace design, operating parameters (e.g., temperature, slag chemistry, specific energy input), and the type of refractory material used.

B. Electrode consumption

Electrode consumption is a high operational cost and an important environmental consideration in electric arc furnace metallurgical processes. The rate of electrode wear is influenced by various factors, including electrical parameters (current, voltage), furnace atmosphere, slag chemistry, operating temperature, and the specific composition of the electrode material itself [34]. Minimizing electrode consumption is crucial for improving the overall economic efficiency and reducing the carbon footprint of ferroalloy production. This section quantifies the electrode consumption during the experimental campaigns and discusses its implications.

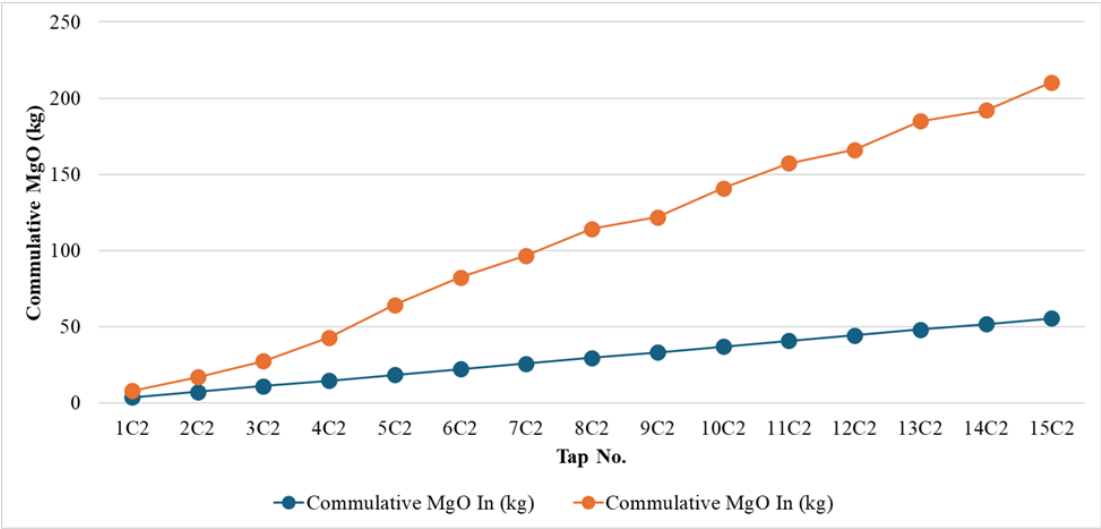
The total mass of electrode consumed during each campaign was measured and then normalized by the total mass of metal produced to derive a specific electrode consumption rate, expressed in kilograms of electrode per kilogram of metal. The results are summarized in Table 15.

Table 15. Electrode consumption rates.

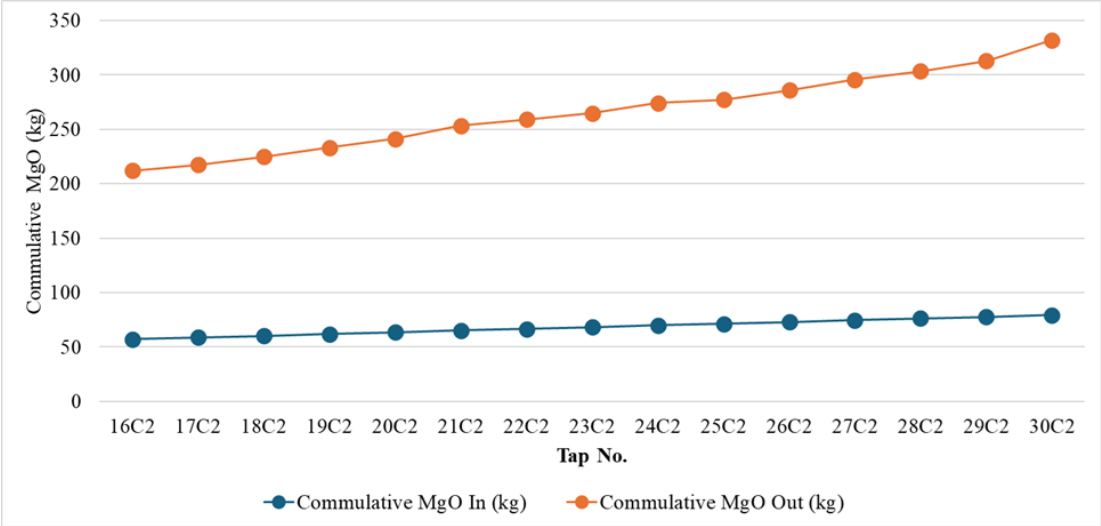
Ore	Tap No.	Mass Electrode Consumed (kg)	Mass Metal Produced (kg)	Electrode Consumption Rate (kg/kg)
UMK	3–10	20	316.89	0.063
UMK/N-Ore	11–22	20	511.27	0.039
N-Ore	23–29	20	377.38	0.053

The specific electrode consumption rates varied considerably across the three experimental campaigns, ranging from a notably low 0.039 kg electrode/kg metal to 0.063 kg electrode/kg metal for the UMK ore pre-reduced in a retort-packed bed furnace. The Nch-

waning ore pre-reduced in a plasma rotary furnace showed an intermediate consumption rate of 0.0596 kg electrode/kg metal.



(**a**)



(**b**)

Figure 13. Refractory consumption during smelting of pre-reduced Mn ores: (**a**) UMK ore pre-reduced in a packed-bed retort furnace, (**b**) Nchwaning ore pre-reduced in a packed-bed retort furnace.

3.1.4. Environmental Impact Assessment: CO_2-Equivalent Emissions per Ton of Product, Dust and Particulate Emissions, NO_x/SO_x Emissions

Environmental impacts were quantified using attributional life-cycle assessment principles in accordance with ISO 14040 [35], ISO 14044 standards [36,37].

The system boundary for this assessment included direct process emissions, as well as indirect emissions associated with electricity generation and reductant production. The functional unit for all impact assessments is defined as one tonne of final alloy product. This evaluation combined direct process emissions measured by an accredited environmental monitoring laboratory with indirect emissions from literature-based estimates.

A. Stack emissions and atmospheric pollutants

Stack monitoring of the 200 kW DC arc furnace was performed by Rayten Engineering Solutions Ltd., an independent laboratory accredited to ISO/IEC 17025:2017 [38] standards by SANAS (T0894) [39]. The measurements were conducted during the June 2025 Mintek

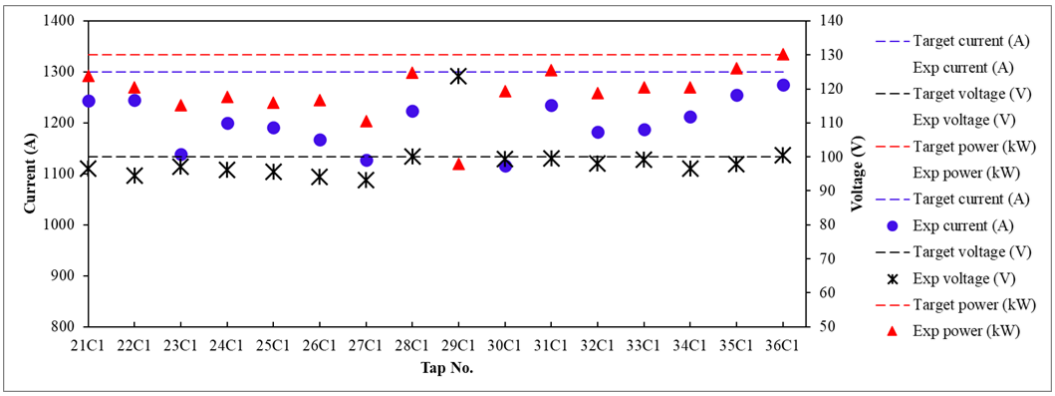
Campaign 2, utilizing internationally accepted reference methods that comply with the National Environmental Management: Air Quality Act of 2004 (Act 39 of 2004), specifically US EPA Methods 1, 2, 3A, 4, 5, 6C, and 7E for the respective pollutants [39]. Sample ports on the stack were utilized for volumetric flow rate and isokinetic measurements [39].

3.2. Comparison of Partial Process Estimate Energy, Materials, and Sustainability Performance During Smelting of Nchwaning Ore Pre-Reduced from Two Pre-Reduction Approaches

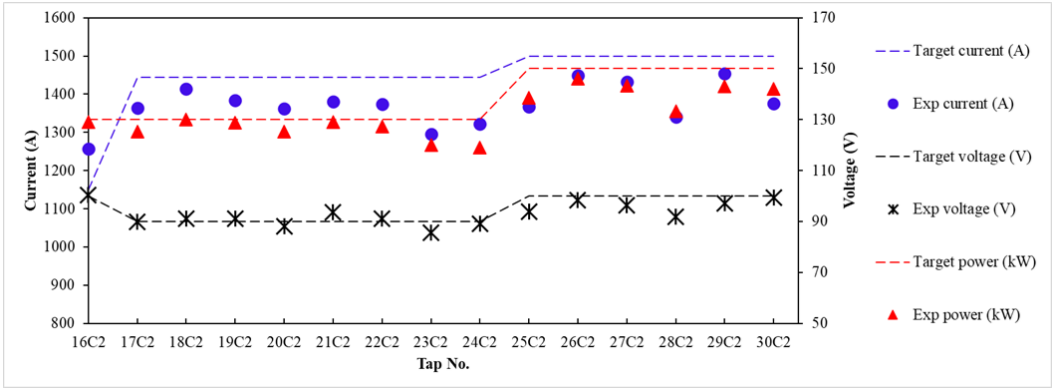
3.2.1. Partial Process Estimate Energy During Smelting of Nchwaning Ore Pre-Reduced from Two Pre-Reduction Approaches

A. Power Stability Metrics: Arc stability, voltage/current fluctuations

Figure 14 shows the comparison of the set-points (current, voltage, and power) against experimentally observed values for the (a) Nchwaning ore pre-reduced in a rotary plasma furnace, and (b) Nchwaning ore pre-reduced in a packed-bed retort furnace.



(**a**) Rotary plasma furnace N-Ore power stability metrics



(**b**) Retort-packed bed furnace N-Ore power stability metrics

Figure 14. Power stability metrics during smelting of pre-reduced Mn ores: (**a**) Nchwaning ore pre-reduced in a rotary plasma furnace, (**b**) Nchwaning ore pre-reduced in a packed-bed retort furnace.

B. Load factor/power-on time

The calculated operational metrics for each pre-reduced manganese ore are summarized in Table 16.

Table 16. Summary of calculated load factors for Mn ores pre-reduced via rotary plasma and vertical retort pre-reduction approaches.

Pre-Reduction Approach	t_{smelt} (h)	t_{down} (h)	η_{LF} (%)
Nchwaning plasma rotary furnace	42.74	1.37	96.89
Nchwaning retort-packed bed furnace	50.55	1.62	96.89

Both pre-reduction approaches demonstrated a load factor of 96.89%. This indicates a remarkably efficient utilization of the experimental furnace across all tests, characterized by minimal inter-tap downtime.

3.2.2. Comparative Assessment of Smelting Performance of Nchwaning Ore Pre-Reduced by Two Approaches

A. Reductant efficiency

The reductant efficiencies observed for the two approaches employed in this study are shown in Figure 15, and demonstrate variability depending on the specific pre-reduction approach. For Nchwaning manganese ore lumps pre-reduced in a plasma rotary furnace, efficiencies ranged from 28.98% to 75.34%. Nchwaning manganese ore pre-reduced in a retort-packed bed furnace exhibited efficiencies between 30.89% and 55.32%. This can be attributed to the pre-reduction extent of the respective ores via the respective pre-reduction approaches.

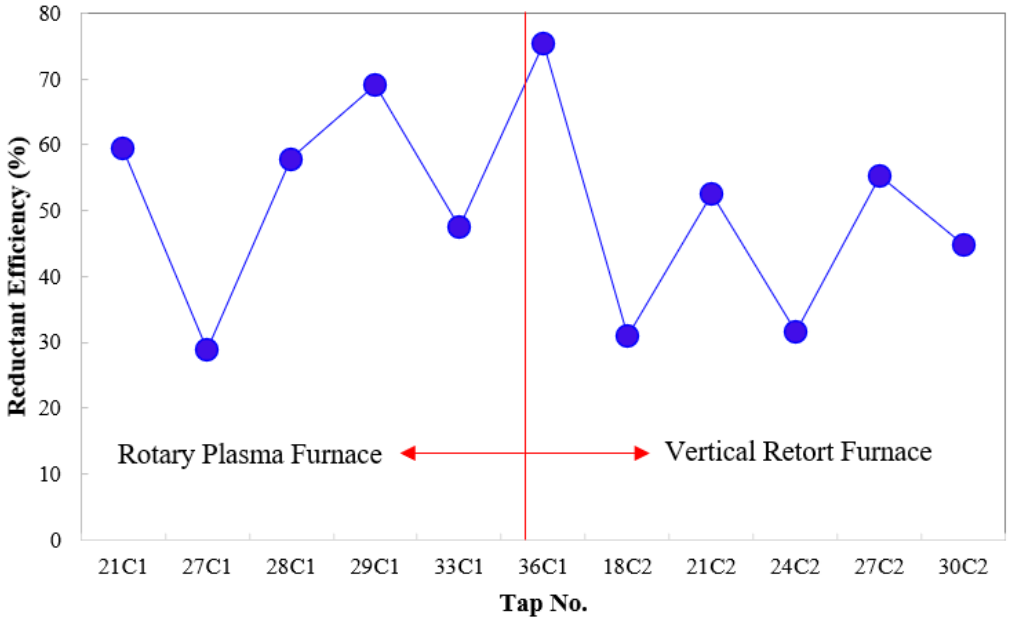


Figure 15. Reductant efficiencies during smelting of manganese ores pre-reduced using two approaches.

B. Slag-to-Metal Ratio

The experimental slag and metal masses obtained in this study (for the two approaches) are given in Table 17, alongside the slag-to-metal ratios. The overall SMRs were 1.34 kg/kg and 1.79 kg/kg for the rotary plasm furnace and vertical retort furnace approaches, respectively. The individual tap-wise SMRs are also presented in Figure 16.

Table 17. Overall slag-to-metal ratios during smelting of Nchwaning ore pre-reduced by two approaches.

Pre-Reduction Approach	Total Slag (kg)	Total Metal (kg)	Overall Slag-to-Metal Ratio (kg/kg)
Rotary Plasma Furnace	1143	638	1.79
Vertical Retort Furnace	944.33	704	1.34

3.2.3. Comparative Assessment of the Refractory and Electrode Consumption During Smelting of Nchwaning Ore Pre-Reduced by Two Approaches

A. Refractory consumption

The refractory consumption for the two approaches, expressed as kilograms of MgO consumed per kilogram of metal produced, are given in Table 18 and in Figure 17.

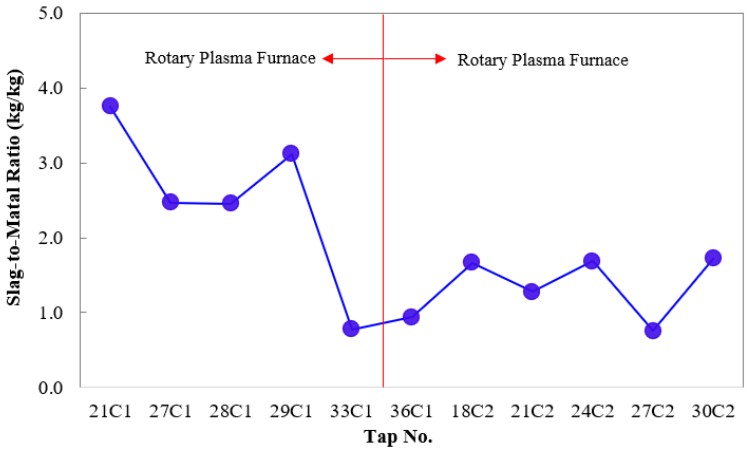
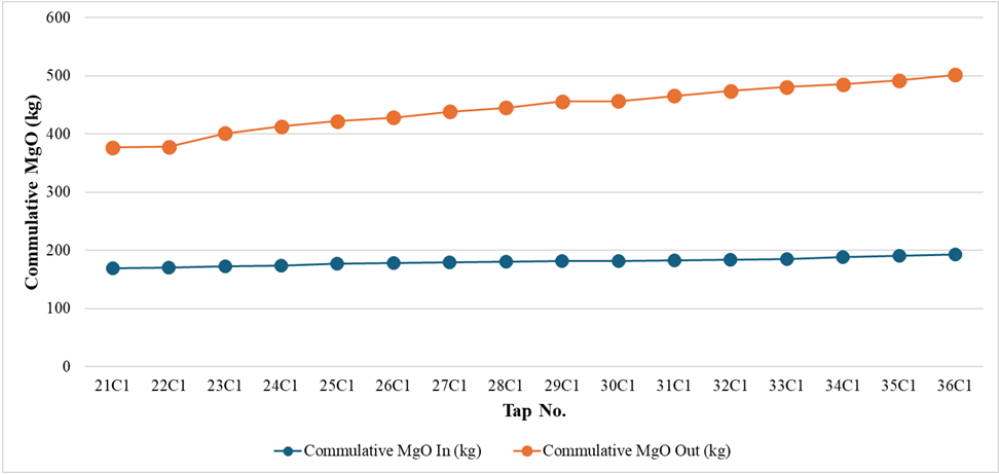


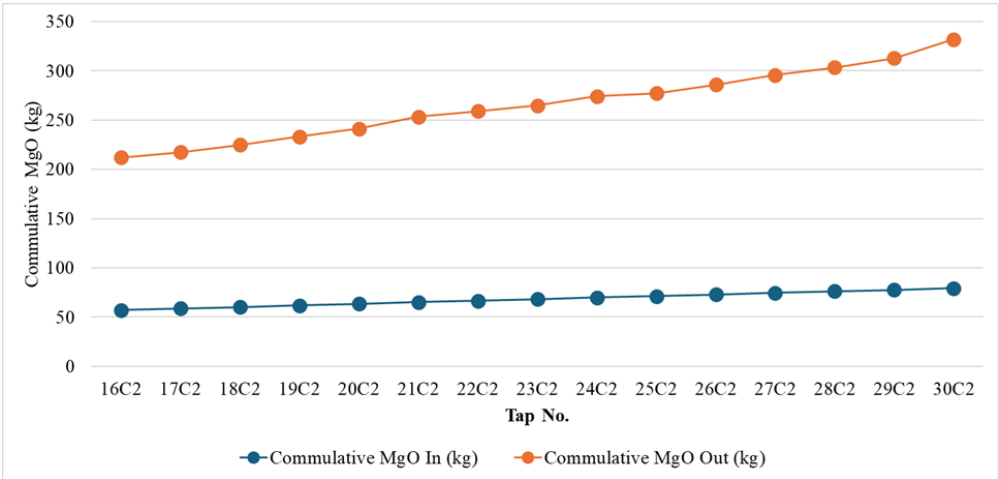
Figure 16. Slag-to-metal ratios during smelting of Mn ores pre-reduced using two approaches.

Table 18. Refractory consumption rates for experimental campaigns.

Pre-Reduction Approach	MgO Consumed (kg)	Metal Produced (kg)	Refractory Consumption Rate (kg MgO/kg Metal)
Rotary Plasma Furnace	117.27	638	0.1838
Vertical Retort Furnace	74.03	704	0.1051



(**a**)



(**b**)

Figure 17. Refractory consumption during smelting of pre-reduced Mn ores: (**a**) Nchwaning ore pre-reduced in a rotary plasma furnace, (**b**) Nchwaning ore pre-reduced in a packed-bed retort furnace.

4. Discussions

4.1. Pre-Reduction Extent

The experimental results for the UMK and Nchwaning ores obtained using the vertical retort furnace, and those for the Nchwaning ore obtained using the plasma rotary furnace, are summarized in Table 8 and Table 9, respectively. From the vertical retort furnace pre-reduction tests, a total of 31 pre-reduction tests were performed (16 on UMK and 15 on N-ore), utilizing a combined raw ore input of 3727 kg. The large-scale pre-reduction campaign, involving over 3700 kg of raw ore, demonstrates the industrial scalability of hydrogen-mediated conditioning. From the plasma rotary furnace pre-reduction tests, the respective three campaigns yielded 270.0 kg pre-reduced lumps (from 317.7 kg raw lumps), 436.5 kg pre-reduced lumps (from 500.0 kg raw lumps), and 519 kg pre-reduced lumps.

The VRF process consumed 670.2 kg of Ar and 135.6 kg of H_2, resulting in the production of 1622 kg of pre-reduced UMK and 1618 kg of pre-reduced N-ore for the subsequent smelting–aluminothermic reduction stage. The high argon consumption highlights the critical requirement for maintaining an inert atmosphere to prevent the re-oxidation of *MnO* and metallic iron during the cooling and discharging phases.

The plasma rotary furnace achieved a maximum reduction of 34.37% for Nchwaning ore at 10 h, outperforming the VRF results for the same ore type. This enhanced efficiency is likely due to the high energy flux of the plasma system and the improved gas–solid contact inherent in a rotary kiln. However, the fluctuations in reduction degree observed between 12 and 15 h (25.81–29.05%) suggest a kinetic threshold.

A notable observation in the vertical retort furnace trials was the greater extent of reduction achieved by UMK ore (67.61%) compared to Nchwaning ore (34.53%), despite Nchwaning's longer residence time. This performance gap is largely explained by the distinct mineralogy of the Kalahari Manganese Field ores. UMK is a carbonate-rich ore, and literature confirms that hydrogen significantly accelerates the decomposition of carbonates compared to carbon monoxide-based atmospheres. The rapid mass loss in UMK is attributed to this expedited carbonate removal and the more complete metallization of iron oxides in pure H_2 environments [2,40].

In contrast, Nchwaning ore primarily consists of higher-grade oxides like braunite I and II [16]. While H_2 facilitates the conversion of Mn_2O_3 to MnO and Fe_2O_3 to metallic iron, the kinetics are highly temperature-sensitive [13]. The target temperature of 750 °C for Nchwaning in the VRF may have limited the reduction rate compared to the 800 °C employed for UMK, as H_2 reduction rates have been shown to increase significantly with every 100 °C increment [6].

Literature indicates that at temperatures between 700 and 900 °C, Nchwaning ore particles undergo significant microstructural changes, including a notable reduction in BET surface area and pore volume due to sintering [6]. This sintering can encapsulate unreacted oxides, restricting H_2 diffusion to the gas–solid interface and potentially explaining why extended residence times in the PRF did not yield progressively higher reduction values [6,13].

These results confirm that H_2 pre-reduction can effectively lower the oxidation state of the feed before the smelting–aluminothermic stage, which is essential for reducing the consumption of expensive aluminum reductants and lowering the carbon footprint of ferromanganese production [13].

4.2. Discussion of Partial Process Estimate Energy During Smelting in a 200 kW DC Arc Furnace Facility

4.2.1. Power Stability Metrics: Arc Stability, Voltage/Current Fluctuations

Despite furnace electric arc stability, voltage and current being critical operational indicators, the deviations between target and experimental values are inherent to electric arc furnace operations and reflect the dynamic nature of the arc, the varying charge characteristics, and the control system's response [41,42]. The observed fluctuations (in Figure 14) are a direct indication of arc instability, which can also be influenced by factors such as arc movement and plasma jet length variations [43,44].

Critically, voltage instabilities and voluntary voltage reduction directly affect power stability and reduce delivered power [10,45]. In this experimental framework, initial arc instability at 100 V necessitated a reduction in target voltage to 70 V for some trials with UMK ore, indicating a necessary operational adjustment to maintain a stable process and avoid excessive fluctuations. Control systems in many EAF operations aim to minimize variations in arc voltage and current to maximize power input and stabilize the process [42,46].

Large and frequent deviations and transients are known to increase electrode erosion significantly [47]. This occurs through enhanced oxidation at hot spots during arc wandering, mechanical tip wear during electrode slipping and re-striking, and localized hot-spot evaporation or chemical attack of the electrode and refractory lining [47]. The impact on refractory life is also pronounced, as arc wandering and poor heat coupling increase local refractory heating, which can shorten the lining's operational lifespan [47]. High voltage and current fluctuations are also associated with increased wear on furnace components and higher energy losses [45].

Arc stability in EAFs is not typically measured by a single universal efficiency percentage. Instead, it is often quantified using statistical indices of voltage and current signals, such as standard deviation, variance, or specific power factor ranges [48,49]. High voltage and current fluctuations indicate a less stable arc, leading to erratic heat transfer and higher energy losses [45].

Researchers have proposed various metrics and models, including the Arc Quality Index, to evaluate arc quality and stability [50]. In this study, power stability in a DC arc furnace is assessed using three complementary, quantitative metrics, namely, current-tracking error (percentage deviation between measured and set-point current), voltage deviation (percentage deviation between measured and set-point voltage), and realized power deviation (percentage deviation between measured and target active power).

These quantitative metrics can be defined by

$$\Delta I_{\%} = \frac{I_{\text{exp}} - I_{\text{set}}}{I_{\text{set}}} \times 100\%, \tag{11}$$

$$\Delta V_{\%} = \frac{V_{\text{exp}} - V_{\text{set}}}{V_{\text{set}}} \times 100\%, \tag{12}$$

$$\Delta P_{\%} = \frac{P_{\text{exp}} - P_{\text{set}}}{P_{\text{set}}} \times 100\%. \tag{13}$$

These metrics together quantify the closeness of the operator setpoints and the degree of transient disturbances that can increase electrode wear and refractory attack [20]. The observed statistics, indicating a systematic shortfall of realized current and power relative to set-points (mean deviations approximately −10% to −12%) with moderate shot-to-shot variability (standard deviations 4% to 6%), can be attributed to factors such as arc instabilities, occasional electrode slipping/immersion transients that reduce effective current

transfer, variations in bath impedance during feed events, and voltage reduction initiated by unstable arc conditions [51].

4.2.2. Specific Energy Requirement

The specific energy requirement (SER) is influenced by a range of operational factors, including voltage and power adjustments [52], targeted SER setpoint changes, the addition of reductants and fluxes (such as lime, coke, and oxygen) [21,53], transitions in ore type [21,54], and variations in feed rate [25]. Therefore, operational adjustments, such as reducing the voltage from 100 V to 70 V to stabilize power delivery following initial arc instability, and subsequently increasing the power (from 130 to 150 kW) and the voltage (to 100 V), had a direct impact on the total energy input and, consequently, the calculated SER.

For high-carbon ferromanganese production in submerged arc furnaces, typical specific energy requirements range between 2.0 and 3.5 MWh per tonne of alloy [27]. The innovative HAlMan process, which leverages smelting–aluminothermic reduction, has demonstrated the potential for substantially lower specific energy requirement values. Reported figures indicate values around 880 kWh/tonne for similar eco-friendly, low-carbon manganese ferroalloy production methods, representing a significant energy reduction compared to conventional processes [55]. This aligns with findings where pre-treated materials can lead to over 50% reduction in electricity demand for HCFeMn production [56]. The current SER values, ranging from 0.8 to 1.15 kWh/kg (equivalent to 800–1150 kWh/tonne), fall within a competitive range, particularly when considering the aluminothermic nature of the process [12,57,58].

4.2.3. Load Factor/Power-On Time

The observed high load factors (95.89% and 96.89% for Nchwaning and UMK ores, respectively) align well with the inherent operational flexibility and process control advantages offered by DC arc furnace technology, which often translates to higher furnace availability and lower heat losses during operation compared to other furnace types. Such high operational continuity is highly advantageous in industrial settings, suggesting that these smelting routes, particularly when coupled with efficient material handling, can achieve superior productivity. Industrial electric arc furnaces, particularly in sectors such as steelmaking and ferroalloy production, target high utilization rates to maximize throughput and cost-effectiveness. For instance, the average capacity utilization factor for scrap-based EAFs in the EU has been reported to be around 83% [59].

For the UMK ore, it is notable that one tap (Tap No. 1C2) registered 0.0 h tap duration, which might indicate a non-operational or aborted run. While this specific instance would contribute to downtime if it were a planned part of the cycle, its impact on the overall load factor, given the very low summed t_{down} values, suggests that the typical operational flow between taps was very efficient.

4.3. Discussion of Alloy and Slag Characterization, Reductant Efficiency and Elemental Mass Balance

4.3.1. Discussion of Metal and Slag Compositions

The chemical analysis of the metallic and slag phases (as summarized in Tables 11 and 12, respectively) provides a quantitative measure of the reduction efficiency and phase partitioning during the smelting of Nchwaning and UMK manganese ores. The metallic phase produced in this study is characterized by high manganese concentrations (61.90–77.33 wt.%) and exceptionally low carbon content (0.15–0.66 wt.%). This composition deviates significantly from standard High Carbon Ferromanganese, which typically contains 7–8% carbon [27]. Instead, the results align with the production of Medium or Low Carbon Ferromanganese (MCFeMn/LCFeMn). The high iron content (up to

40.01 wt.%) in samples such as 2C2 is indicative of the ferruginous nature of Nchwaning ore, which has a lower Mn/Fe ratio compared to other high-grade ores like Comilog [27]. These alloy specifications are consistent with the HAlMan process benchmarks reported by Sarkar et al. [13], where hydrogen-based reduction facilitates the production of low-carbon alloys by bypassing the traditional coke-intensive carburization stage.

The transition of MnO from the initial slag (58.9% in 1C2) to the final stages (12.45% in 30C2) demonstrates a high degree of manganese recovery. According to Rimal and Tangstad [60], the rate of MnO reduction is typically constant as long as a solid MnO phase is present in the slag, subsequently decreasing as the slag enters the single-phase liquid region. The low residual MnO concentrations observed in samples 12C2 through 15C2 (down to 6.40%) suggest that the smelting conditions achieved high thermodynamic driving forces for reduction.

The slag chemistry is dominated by the quinary MnO-SiO_2-Al_2O_3-CaO-MgO system. A distinctive feature of the experimental slags is the high concentration of Al_2O_3 (up to 52.45%) and CaO (up to 37.5%). As MnO and SiO_2 are reduced into the alloy, non-reducible oxides like Al_2O_3 and CaO concentrate in the slag phase. Tangstad et al. [29] highlight that such high alumina concentrations significantly influence the slag liquidus temperature and viscosity. Furthermore, the presence of high CaO and Al_2O_3 likely promotes the formation of gehlenite ($Ca_2Al[AlSiO_7]$)-type phases, which can stabilize the slag but may also affect the activity of residual MnO, thereby impacting the final metal–slag separation efficiency [28,61].

4.3.2. Reductant Efficiency

The high reductant efficiency (reported in Section 3.1.2) can be associated with factors such as the aluminum content in the charge and critical aspects of slag chemistry [3]. Optimized slag conditions, characterized by carefully controlled basicity, viscosity, and liquidus temperature, are essential for efficient metal–slag separation and high recovery rates of manganese [60,62]. Variations in these parameters can significantly impact the effectiveness of aluminum as a reductant, affecting overall efficiency and metal yield.

Furthermore, process parameters such as pre-reduction methods, furnace design, and the inherent characteristics of the manganese ore (e.g., mineralogy, particle size) play a crucial role in determining reductant efficiency [4,5,63]. Excess aluminum additions, oxidation losses, and the efficiency of recovery in the final alloy also contribute to the overall reductant utilization [64]. Higher efficiency values indicate that a substantial proportion of the added aluminum actively participates in the desired reduction reactions, leading to improved recovery of valuable metals and a reduction in energy consumption [64]. Continuous optimization of these integrated process elements is vital for advancing sustainable and economically viable manganese production [12,30].

4.3.3. Elemental Accountability

The observed deviations from 100% accountability can be attributable to a combination of experimental and analytical uncertainties. These can include significant measurement errors, material heterogeneity, and sampling errors during the characterization of inputs and outputs [65,66]. Incomplete recovery of fine particles, minor losses through volatilization, or unquantified dust streams can also contribute to these discrepancies [67]. Such challenges are common in high-temperature metallurgical processes, where precise measurement of flows and concentrations can be sparse [66], and the incorporation of an uncertainty model is crucial for a realistic evaluation of mass balance reliability [67,68]. For instance, uncertainties in raw material composition and weighing,

as well as element distribution factors, are known to influence mass balance closure in industrial operations [69].

The accountability results are consistent with literature observations for similar pyrometallurgical reduction systems, where acceptable mass balance closures typically fall within ±10% [3]. Industrial smelting operations often report elemental accountabilities between 90% and 110% due to inherent process heterogeneity, complex phase interactions, and practical sampling constraints [7]. Therefore, the values obtained in this study confirm the reliability of the mass balance and validate the analytical methodology used for subsequent recovery and deportment analyses.

4.3.4. Elemental Recovery

The high recoveries for Mn and Fe suggest favorable thermodynamic conditions for their reduction and subsequent capture in the metallic phase. The relatively lower Si recovery indicates that a significant portion remained in the slag phase, which is expected due to its higher stability in oxide form under certain conditions. The presence of Al recovery, even if minor, suggests its co-reduction or entrapment, influenced by the reductant used and reaction temperature.

These findings are consistent with recent studies on manganese and aluminum recovery via high-temperature smelting–aluminothermic reduction processes [3,70]. The HAlMan process, for instance, highlights efficient Mn and Al-Mn alloy production through hydrogen pre-reduction followed by smelting–aluminothermic reduction, aiming for low energy consumption and carbon footprint [12,57].

Comparatively, the literature reports for smelting–aluminothermic reduction or carbothermic smelting of manganese alloys show Fe and Mn recoveries typically between 85 and 95% under optimized industrial conditions. The recoveries obtained in this study, especially for Fe and Mn, fall within or approach this range, confirming that the process achieved near-industrial efficiency for the primary target metals despite the use of secondary aluminum as the reductant. The overall recovery data aligns with expectations for such processes and underscores the impact of process conditions and pre-reduction methods, such as hydrogen-based pre-reduction of ferromanganese oxides [9], on overall process efficiency.

Overall, the recovery data validate the process performance and demonstrate that the reduction pathway effectively transferred target metals into the alloy phase while maintaining acceptable slag compositions for subsequent handling or recycling.

4.3.5. Elemental Deportment

The observed deportment patterns confirm the strong reducibility and affinity of Fe and Mn for alloy formation, leading to their preferential partitioning into the metal phase. The high concentration of Al in the slag indicates that this element predominantly remained in its oxide form, aligning with its thermodynamic stability under the experimental conditions.

The substantial deportment of Si to the metal phase suggests effective co-reduction of silica under these process parameters. This selective partitioning is a key aspect of element distribution in silicomanganese production processes, where pilot-scale studies confirm the distribution of minor and trace elements across product streams [71]. Minimal dust losses generally signify efficient capture within the primary phases. Moreover, in the smelting–aluminothermic reduction, there is no gas generation via the chemical reactions, and hence the transport of fine particles is minimal due to more natural convection.

The deportment behavior observed here agrees with reported findings for smelting–aluminothermic reduction of manganese and iron oxides, where Fe and Mn exhibit preferential reduction and metallic enrichment, while Al, Si, and Ca (if present) remain slag-

associated [3,70]. The effective partitioning of Mn and Fe into the metal phase and the confinement of Al and a significant portion of Si in the slag phase (though less for Si in this overall data) indicate effective process selectivity and minimal contamination of the metallic product. Studies on slag properties in ferroalloy production further elucidate these phase distributions [5,29].

The deportment results demonstrate that the process achieved stable and predictable phase separation, with elemental distributions consistent with thermodynamic predictions and industrial benchmarks. This confirms the reproducibility and robustness of the reduction–tapping sequence for alloy recovery.

4.3.6. Slag-to-Metal Ratio

The ratio of slag to metal is an important measure of how efficient and sustainable manganese ferroalloy manufacturing is, especially in the HAlMan process. The SMRs for industrial high-carbon ferromanganese production using submerged arc furnaces are usually between 1.0 and 1.6 kg/kg; these numbers might change depending on the grade of the ore and the conditions under which it is being worked. The HAlMan method, which uses smelting–aluminothermic reduction, shows competitive SMRs. For example, the Nchwaning ore (retort-packed bed) has an SMR of 1.34 kg/kg, which is in line with or even higher than the upper end of usual industrial ranges. Aluminothermic methods naturally make alumina-rich slag. The exact SMR depends on how much reductant is used and the stoichiometry of the reaction. One of the main benefits of employing pre-reduced manganese ores, as this study does, is that it lowers the overall volume of slag compared to smelting raw ores. This results in lower SMRs and better energy efficiency. It is worth noting that more optimization of the process and reaching high Mn yields will reduce the slag mass and increase the metal mass, and hence lower the SMR.

A favorable SMR has a big impact on both the cost of the process and the way waste is handled. A lower SMR means that fewer raw materials are used, less energy is needed to melt and heat the slag, and the furnace works better since it can process more metal. From an environmental point of view, reducing slag production directly lowers disposal costs and makes the operation more sustainable, which is important because of increased regulatory pressure on solid waste management. Changes in the pre-reduction approach and how the plant runs also affect the SMRs that are seen. For instance, Nchwaning ore that was pre-reduced in a retort-packed bed furnace had a lower SMR (1.34 kg/kg) than the same ore that was pre-reduced in a plasma rotary furnace (1.79 kg/kg). To obtain the best metal recovery and SMR, it is important to change operational parameters, such as adding aluminum and changing the chemistry of the slag. The study shows that pre-reducing manganese ore, especially Nchwaning ore in a packed-bed retort furnace, can lead to competitive SMRs. This means that there is room for additional optimization to improve both economic and environmental performance.

4.4. Discussion of Operations Sustainability: Refractory and Electrode Consumption

4.4.1. Refractory Consumption

Refractory consumption rates in experimental campaigns ranged from 0.1051 to 0.1838 kg MgO/kg metal, influenced by furnace design, operating parameters like temperature and slag chemistry, and the refractory material itself. Minimizing refractory wear is crucial in industrial ferroalloy production due to its impact on costs and campaign life. While specific figures for experimental manganese ferroalloy smelting are scarce, general industry benchmarks for electric arc furnace operations, especially with aggressive slags, highlight the challenge of refractory degradation. DC arc furnaces, like the one used in this study, offer flexibility but can also contribute to refractory erosion due to intense localized

heat and stirring. The observed refractory consumption rates have significant implications for the HAlMan process's economic viability and operational stability. Lower consumption directly reduces material and labor costs associated with maintenance. Slower wear extends furnace campaign life, improving availability and productivity by reducing shutdowns. Consistent refractory wear also contributes to more stable furnace operation, mitigating risks of failures. These differences in consumption are linked to the pre-reduction approach and slag characteristics, with slag chemistry and basicity being a major factor. Aggressive slag components can accelerate refractory dissolution, suggesting that a lower SMR and corresponding lower consumption, as seen with Nchwaning ore, likely resulted from a less aggressive slag composition or a more stable slag–refractory interface.

4.4.2. Electrode Consumption

The specific electrode consumption rates varied considerably across the three experimental campaigns, ranging from a notably low 0.039 kg electrode/kg metal to 0.063 kg electrode/kg metal for the UMK ore pre-reduced in a retort-packed bed furnace. The Nchwaning ore pre-reduced in a plasma rotary furnace showed an intermediate consumption rate of 0.0596 kg electrode/kg metal.

Electrode consumption rates in industrial ferroalloy production are typically higher than those observed in steelmaking EAFs due to the more aggressive nature of ferroalloy slags and often longer processing times. In the HAlMan process, there is no CO_2 gas formation in the smelting–aluminothermic reduction furnace, and therefore, there is no electrode consumption via the Boudouard reaction at elevated temperatures, which is a mechanism of graphite electrode consumption in the ferroalloys furnaces.

While precise, universally comparable figures for electrode consumption in laboratory or pilot-scale DC EAFs for ferromanganese are not readily available, for high carbon ferromanganese production in submerged arc furnaces, energy consumption typically ranges from 2.0 to 3.5 MWh per tonne of alloy [5]. Electrode consumption is a component of overall production cost, and reducing it is a continuous goal in the industry [72]. Using manganese blends with a higher Mn/Fe ratio can reduce coke consumption, which in turn can lead to reduced electrode consumption [73].

4.5. Discussion of Environmental Indicators: CO_2-Equivalent Emissions per Ton of Product, Dust andParticulate Emissions, NO_x/SO_x Emissions

4.5.1. Stack Emissions and Atmospheric Pollutants

The summary of measured stack gas parameters for the 200 kW DC arc furnace during HAlMan process Campaign 2 operation has shown a CO_2 concentration of 775 mg/Nm^3, which represents ambient background levels, not a process emission from the furnace [39]. The observed high oxygen content (20.8 %v/v) indicates oxidizing off-gas conditions and minimal formation of reducing gases such as CO, which was measured at 0 mg/Nm^3 [39]. These values are well below typical industrial thresholds, indicating a low atmospheric impact; however, no specific regulatory limits were compared against as this was the first run of the process [39].

Assuming a representative volumetric flow rate of 1200 Nm^3 h^{-1} and an alloy production rate of 10 kg h^{-1}, the corresponding mass emission rates and emission factors were calculated. These translate to emission factors of 26 kg PM, 0.8 kg SO_2, 2.4 g NO_x, and 0.34 kg CO per tonne of alloy. Compared with typical values for conventional carbothermic HCFeMn smelting (PM 1–3 kg t^{-1}, SO_2 0.3–0.8 kg t^{-1}, NO_x 0.2–0.6 kg t^{-1}; [7,74]), the HAlMan process exhibits a substantially lower gaseous emission intensity and a cleaner overall profile.

4.5.2. Greenhouse-Gas Emissions

Direct CO_2 emissions from the furnace are negligible owing to the absence of carbon reductants. The total CO_2-equivalent impact, therefore, consists of indirect contributions from electricity generation and aluminum reductant production:

$$E_{CO_2,\,\mathrm{total}} = E_{\mathrm{elec}} + E_{\mathrm{Al\text{-}prod}}. \tag{14}$$

For a specific energy consumption of 1500 kWh t^{-1} and a South African grid emission factor of 0.8 kg CO_2 kWh^{-1}, the electricity-related contribution (E_{elec}) is calculated as 1.20 t CO_2-eq t^{-1}. Assuming 0.30 t Al t^{-1} alloy and an embodied carbon intensity of 0.5 kg CO_2 kg^{-1} for recycled aluminum, the aluminum production contribution ($E_{\mathrm{Al\text{-}prod}}$) is 0.15 t CO_2-eq t^{-1}. This gives a total CO_2-equivalent impact of 1.35 t CO_2-eq t^{-1}.

This represents a 60–65% reduction compared with the 3–4 t CO_2-eq t^{-1} typical of carbothermic HCFeMn production [7,74]. The choice of electricity source and the use of recycled aluminum significantly influence the overall carbon footprint of metallurgical processes [75,76].

4.5.3. Aggregate Environmental Load

To express a single environmental-load index, the individual impact categories were weighted following the approach of Refs. [77,78], employing ReCiPe midpoint normalization (Equation (15)). The specific weighting factors (w_1, w_2, w_3, and w_4) correspond to the relative environmental relevance of each category (CO_2, SO_2, NO_x, and PM, respectively).

$$E_{\mathrm{load}} = w_1 E_{CO_2} + w_2 E_{SO_2} + w_3 E_{NO_x} + w_4 E_{\mathrm{PM}}, \tag{15}$$

where weighting factors $w_1 = 1.0$, $w_2 = 0.25$, $w_3 = 0.30$, and $w_4 = 0.05$ correspond to the relative environmental relevance of each category (ReCiPe midpoint normalization). The resulting aggregate impact for the HAlMan process is dominated by indirect CO_2 emissions, while contributions from acidifying and particulate pollutants remain minor.

4.6. Comparative Discussion of Smelting Performance of Nchwaning Ore Pre-Reduced by Two Approaches: Partial Process Estimate Energy, Material, and Sustainability Performance During Smelting

4.6.1. Comparative Discussion of Partial Process Estimate Energy During Smelting of Pre-Reduced Manganese Ores

A. Power Stability Metrics: Arc stability, voltage/current fluctuations

Figure 14 shows the comparison of the set-points (current, voltage, and power) against experimentally observed values for the (a) Nchwaning ore pre-reduced in a rotary plasma furnace, (b) UMK ore pre-reduced in a packed-bed retort furnace, and (c) Nchwaning ore pre-reduced in a packed-bed retort furnace.

Deviations between target and experimental values are inherent to electric arc furnace operations and reflect the dynamic nature of the arc, the varying charge characteristics, and the control system's response [41,42]. The observed fluctuations (in Figure 14) are a direct indication of arc instability, which can also be influenced by factors such as arc movement and plasma jet length variations [43,44].

Critically, voltage instabilities and voluntary voltage reduction directly affect power stability and reduce delivered power [10,45]. In this experimental framework, initial arc instability at 100 V necessitated a reduction in target voltage to 70 V for some trials with UMK ore, indicating a necessary operational adjustment to maintain a stable process and avoid excessive fluctuations. Control systems in many EAF operations aim to

minimize variations in arc voltage and current to maximize power input and stabilize the process [42,46].

Large and frequent deviations and transients are known to increase electrode erosion significantly [47]. This occurs through enhanced oxidation at hot spots during arc wandering, mechanical tip wear during electrode slipping and re-striking, and localized hot-spot evaporation or chemical attack of the electrode and refractory lining [47]. The impact on refractory life is also pronounced, as arc wandering and poor heat coupling increase local refractory heating, which can shorten the lining's operational lifespan [47]. High voltage and current fluctuations are also associated with increased wear on furnace components and higher energy losses [45].

Arc stability in EAFs is not typically measured by a single universal efficiency percentage. Instead, it is often quantified using statistical indices of voltage and current signals, such as standard deviation, variance, or specific power factor ranges [48,49]. High voltage and current fluctuations indicate a less stable arc, leading to erratic heat transfer and higher energy losses [45].

Researchers have proposed various metrics and models, including the Arc Quality Index, to evaluate arc quality and stability [50]. In this study, power stability in a DC arc furnace is assessed using three complementary, quantitative metrics, namely, current-tracking error (percentage deviation between measured and set-point current), voltage deviation (percentage deviation between measured and set-point voltage), and realized power deviation (percentage deviation between measured and target active power).

These quantitative metrics can be defined by

$$\Delta I_{\%} = \frac{I_{\text{exp}} - I_{\text{set}}}{I_{\text{set}}} \times 100\%, \tag{16}$$

$$\Delta V_{\%} = \frac{V_{\text{exp}} - V_{\text{set}}}{V_{\text{set}}} \times 100\%, \tag{17}$$

$$\Delta P_{\%} = \frac{P_{\text{exp}} - P_{\text{set}}}{P_{\text{set}}} \times 100\%. \tag{18}$$

These metrics together quantify how closely the furnace follows operator setpoints and the degree of transient disturbances that can increase electrode wear and refractory attack [20]. The observed statistics, indicating a systematic shortfall of realized current and power relative to set-points (mean deviations approximately −10% to −12%) with moderate shot-to-shot variability (standard deviations 4% to 6%), can be attributed to factors such as arc instabilities, occasional electrode slipping/immersion transients that reduce effective current transfer, variations in bath impedance during feed events, and voltage reduction initiated by unstable arc conditions [51].

B. Load factor/power-on time

All experimental campaigns, including both the Nchwaning manganese ore lumps pre-reduced in a plasma rotary furnace and the UMK and Nchwaning ores pre-reduced in retort-packed bed furnaces, demonstrated exceptionally high load factors, ranging from approximately 95.89% to 96.89%. This indicates a remarkably efficient utilization of the experimental furnace across all tested pre-reduction routes, characterized by minimal inter-tap downtime. Such high operational continuity is highly advantageous in industrial settings, suggesting that these smelting routes, particularly when coupled with efficient material handling, can achieve superior productivity. This performance aligns with the inherent operational flexibility and process control advantages offered by DC arc furnace technology, which often translates to higher furnace availability and lower heat losses during operation compared to other furnace types.

For the UMK ore, it is notable that one tap (Tap No. 1C2) had a tap duration of 0.0 h, which may indicate a non-operational or aborted run. While this specific instance would contribute to downtime if it were a planned part of the cycle, its impact on the overall load factor, given the very low summed t_{down} values, suggests that the typical operational flow between taps was very efficient. The very high load factors observed for the retort-packed bed furnace campaigns indicate that the downtime associated with cooling, material discharge, and subsequent reloading, although inherent to batch processes, was managed very effectively in these experimental setups, resulting in minimal idle periods. While pilot-scale experimental facilities typically experience more frequent interruptions for process adjustments, sampling, and maintenance compared to optimized industrial plants [33,79], the consistently high load factors observed across all campaigns suggest robust operational management during these trials.

Industrial electric arc furnaces, particularly in sectors such as steelmaking and ferroalloy production, target high utilization rates to maximize throughput and cost-effectiveness. For instance, the average capacity utilization factor for scrap-based EAFs in the EU has been reported around 83% [59].

The high load factors achieved in all experimental campaigns, notably exceeding typical industrial averages, suggest a strong potential for industrial scaling and commercial viability for these manganese production routes. This indicates that the operational aspects, at least in terms of furnace availability and minimized idle time, are highly favorable. High downtime, conversely, leads to significant economic penalties due to lost production and sustained energy losses from refractory linings in intermittent operations [80].

The presented load factors underscore that the choice of pre-reduction approach, while influencing chemical and metallurgical efficiencies, was implemented in a manner that ensured high operational continuity in the subsequent smelting process. This operational analysis provides crucial quantitative data for comprehensive techno-economic assessments and informs strategic decisions regarding the industrial scalability and commercial viability of these novel manganese production routes. Future work might focus on maintaining these high load factors during scale-up to larger industrial operations, considering the challenges associated with managing larger material volumes and more complex operational logistics.

4.6.2. Comparative Discussion of Smelting Performance of Nchwaning Ore Pre-Reduced by Two Approaches: Alloy and Slag Characterization, Reductant Efficiency and Elemental Mass Balance

A. Reductant efficiency

The reductant efficiencies observed in this study (as shown in Figure 15) demonstrate variability depending on the specific pre-reduction method and ore type. For Nchwaning manganese ore lumps pre-reduced in a plasma rotary furnace, efficiencies ranged from 28.98% to 75.34%. When UMK manganese ore was pre-reduced in a retort-packed bed furnace, the efficiencies spanned from 19.46% to 56.67%.

The complete reduction of manganese oxide via the aluminothermic process is fundamentally influenced by factors such as the aluminum content in the charge and critical aspects of slag chemistry [3]. Variations in these parameters can significantly impact the effectiveness of aluminum as a reductant, affecting overall efficiency and metal yield.

Nchwaning manganese ore pre-reduced in a retort-packed bed furnace exhibited efficiencies between 30.89% and 55.32%. This can be attributed to the pre-reduction extent of the respective ores via the respective pre-reduction approaches.

The process was implemented at elevated temperatures, and the charged aluminum metal was exposed to air for some time before the start of reduction reactions, which may

oxidize a portion of the aluminum metal, and hence reduce the redundant efficiency. Hence, using a protective gas may provide higher reduction efficiency.

B. Slag-to-Metal Ratio

Comparing these values to industrial and literature benchmarks reveals insights into the efficiency of the HAlMan process.

- *Industrial High Carbon Ferromanganese Production:* Conventional industrial HCFeMn production via submerged arc furnaces typically operates with SMRs in the range of 1.0 to 1.6 kg/kg, although values can vary depending on ore quality, furnace type, and operating practices [81]. The HAlMan process, which utilizes smelting–aluminothermic reduction, has been benchmarked for its eco-efficiency against industrial carbothermic HCFeMn production, with positive findings regarding energy consumption and emissions. The reported SMRs in this study, particularly the 1.34 kg/kg for Nchwaning ore (retort-packed bed), fall within or are competitive with the upper end of typical industrial ranges for HCFeMn.
- *Aluminothermic Reduction:* Aluminothermic processes, by their nature, can generate significant amounts of alumina-rich slag. The specific SMR for smelting–aluminothermic reduction largely depends on the reductant usage, slag former additions, and overall process stoichiometry. Generally, processes aiming for high metal recovery might produce more slag to ensure efficient separation and impurity removal. It is worth noting that the obtained slag byproduct is valuable and consumable and can be utilized for smelter-grade alumina production for the primary aluminum production.
- *Pre-reduced Ores:* The use of pre-reduced manganese ores, as in this study, is expected to reduce the overall slag volume compared to smelting raw ores, as a significant portion of oxygen has already been removed. This should inherently contribute to lower SMRs and improved energy efficiency.

Implications for Process Economics and Waste Management:

The SMR directly impacts the economic and environmental sustainability of the process:

- *Process Economics:* A lower SMR leads to several economic advantages:
  - *Reduced Raw Material Consumption:* Less slag formers are required, decreasing raw material costs.
  - *Lower Energy Demand:* Less slag to melt and heat reduces specific energy consumption per unit of metal produced.
  - *Increased Furnace Productivity:* A lower slag volume allows for a higher throughput of metal, improving furnace capacity utilization.
- *Waste Management:* Slag generation is a major waste stream in ferroalloy production. A lower SMR translates directly to:
  - *Reduced Slag Disposal Costs:* Significant cost savings on landfilling or further processing of slag.
  - *Lower Environmental Impact:* Minimizing solid waste contributes to a more sustainable operation and addresses increasing regulatory pressures. Studies highlight the importance of characterizing and valorizing metallurgical slags to reduce environmental impact and conserve resources.

Relationship to pre-reduction approach and operational adjustments:

The observed SMRs can be related to the choice of pre-reduction technology and operational parameters:

- Pre-reduction approach:
  - *Nchwaning ore pre-reduced in a packed bed vs. Nchwaning ore pre-reduced in a rotary plasma furnace:* The Nchwaning ore pre-reduced in the retort-packed bed furnace yielded a lower SMR (1.34 kg/kg) compared to the same ore pre-reduced in the plasma rotary furnace (1.79 kg/kg). This difference could be attributed to variations in the degree of pre-reduction achieved by each method, or differences in the residual gangue composition and morphology after pre-reduction. A more selective or efficient removal of gangue components during pre-reduction in the retort-packed bed could lead to a cleaner feed for the smelting furnace, thus requiring less slag generation.
  - *UMK:* The UMK ore pre-reduced in the retort-packed bed furnace resulted in the highest SMR (1.87 kg/kg) among all campaigns. This suggests that the specific characteristics of the UMK ore, even after pre-reduction in the retort, might necessitate a higher slag volume during smelting to achieve the desired metal recovery or impurity removal. Ore composition, particularly the ratio of manganese oxides to silica and alumina, heavily influences the required slag volume and composition.
- *Operational Adjustments:* While the provided data does not directly detail SER modulation or specific Al additions per tap, these operational parameters are crucial in influencing SMR.
  - *Aluminum Additions:* In smelting–aluminothermic reduction, the amount of aluminum reductant added directly impacts the quantity and composition of the alumina-rich slag formed. Precise control of Al additions is vital to optimize both metal recovery and SMR.
  - *Slag Chemistry and Basicity:* Adjustments to slag chemistry (e.g., lime or silica additions) to achieve optimal basicity and fluidity for efficient metal–slag separation and impurity removal will directly influence the slag volume and, consequently, the SMR. These adjustments are often fine-tuned based on the specific feed material and desired product quality.

The SMRs achieved in this study demonstrate that manganese ore pre-reduction, particularly with the Nchwaning ore in a packed-bed retort furnace, can lead to competitive SMRs when compared to industrial benchmarks. Further optimization of pre-reduction processes and smelting parameters, especially regarding aluminum utilization and slag chemistry, can further enhance these ratios, driving improved economic and environmental performance.

4.6.3. Comparative Discussion of the Refractory and Electrode Consumption During Smelting of Nchwaning Ore Pre-Reduced by Two Approaches

A. Refractory consumption

Refractory consumption, specifically the loss of magnesia from the furnace lining, was estimated by calculating the difference between the cumulative MgO leaving the system in the slag and the cumulative MgO introduced with the feed materials over each campaign. The results, expressed as kilograms of MgO consumed per kilogram of metal produced, are summarized in Table 18 and in Figure 17.

The refractory consumption rates varied between 0.1051 kg MgO/kg metal and 0.1838 kg MgO/kg metal across the experimental campaigns. Refractory consumption rates are highly dependent on specific furnace design, operating parameters (e.g., temperature, slag chemistry, specific energy input), and the type of refractory material used.

In industrial ferroalloy production, minimizing refractory wear is a continuous objective, given its direct impact on operational costs and campaign life.

- *Ferroalloy Production:* While precise, universally comparable figures for refractory consumption in experimental manganese ferroalloy smelting are scarce, general industry benchmarks for EAF operations, particularly those involving aggressive slags, often highlight the challenge of refractory degradation. For example, specific refractory consumption in steelmaking EAFs can range significantly, but typical values are often targeted below 1 kg/tonne steel. Given the nature of manganese alloys and the typically more aggressive slags, these values might be higher for ferroalloy production.
- *DC Arc Furnaces:* The DC arc furnace used in this study is known for its ability to operate with greater flexibility in terms of raw materials and slag chemistry compared to AC furnaces. However, the intense localized heat and strong stirring action caused by the arc can also contribute to refractory erosion if not properly managed [33]. In ferroalloy furnaces, there is usually a cold burden or frozen slag in contact with the refractory, and therefore, much less refractory interaction occurs in comparison with EAF, in which molten slag is in contact with molten slag.

Implications for Process Economics and Operational Stability:

The observed refractory consumption rates have significant implications for the economic viability and operational stability of the HAlMan process:

- *Cost Reduction:* A lower refractory consumption rate, as achieved with the Nchwaning ore pre-reduced in a retort-packed bed furnace, translates directly into reduced material costs for refractories and decreased labor costs associated with patching and relining the furnace.
- *Increased Furnace Availability:* Slower refractory wear extends furnace campaign life, leading to fewer planned and unplanned shutdowns for maintenance. This improves furnace availability and overall productivity, directly impacting the process's economic performance [80].
- *Operational Stability:* Consistent and predictable refractory wear contributes to more stable furnace operation, reducing the risk of breakouts or other refractory-related failures.

Relationship to pre-reduction approach and operational adjustments:

The differences in refractory consumption rates can be linked to the pre-reduction approach and the resulting slag characteristics:

- *Slag Chemistry and Basicity:* The most significant factor influencing refractory wear in smelting is the chemical interaction between the molten slag and the refractory lining. Higher slag basicity and the presence of certain aggressive components (e.g., highly oxidizing conditions or specific oxides) can accelerate refractory dissolution. The lower SMR for the Nchwaning ore (retort-packed bed) and its corresponding lower refractory consumption suggest that this combination might have produced a less aggressive slag composition or a more stable slag–refractory interface. The specific composition of the slag (e.g., MgO content, silica content) dictates its corrosivity to MgO-based refractories [33].

4.6.4. Comparative Performance of Vertical Retort Furnace Pre-Reduction and Plasma Rotary Furnace

The technical and operational metrics for the two pre-reduction routes are summarized in Table 19. This comparison reveals a significant trade-off between reduction kinetics and downstream operational stability. While the Rotary Plasma Furnace achieved a superior reduction extent for Nchwaning ore (34.37%) due to enhanced gas–solid contact and high

energy flux, the Vertical Retort Furnace provided a more stable feed for the subsequent smelting–aluminothermic stage.

Table 19. Comparison of Vertical Retort Furnace and Rotary Plasma Furnace

Parameter	Vertical Retort Furnace	Rotary Plasma Furnace
Primary Mechanism	Packed-bed, static reduction	Rotary kiln, high energy flux plasma
Max N-ore Reduction Extent (R%)	27.67%	34.37%
Target Temperature	750–800 °C	High-intensity thermal flux
Slag-to-Metal Ratio	1.34 kg/kg	1.79 kg/kg
Refractory Consumption	0.1051 kg MgO/kg metal	0.1838 kg MgO/kg metal
Electrode Consumption	0.0530 kg/kg metal	0.0596 kg/kg metal
Key Advantage	High scalability; minimal electrode wear	Rapid kinetics; improved gas–solid contact

The VRF route yielded a lower slag-to-metal ratio of 1.34 kg/kg compared to 1.79 kg/kg for the plasma route, which suggests that the packed-bed conditioning in the VRF leads to higher overall process efficiency and reduced waste generation at this 200 kW pilot scale.

4.7. Comparative Benchmarking

When benchmarked against industrial carbothermic HCFeMn production, the HAlMan process exhibits substantial improvements in multiple performance indicators: (i) a marked reduction in smelting specific energy consumption, (ii) significantly lower CO_2-equivalent emissions, (iii) precipitously lower NO_x/SO_x stack outputs under the pilot operating conditions, and (iv) superior eco-efficiency indices. These improvements collectively validate the environmental and economic promise of the HAlMan approach for valorising HCFeMn slag.

The pilot results demonstrate a clear smelting energy advantage for the HAlMan route: the measured SER ($\approx$0.88 MWh t^{-1}) is 56–75% lower than the commonly reported SAF benchmarks (2.0–3.5 MWh t^{-1}), reflecting the combined effect of the aluminothermic exotherm and the DC arc furnace configuration. The estimated cradle-to-gate CO_2-intensity ($\approx$1.35 t CO_2-eq t^{-1}) likewise compares favorably with typical carbothermic values ($\approx$3–4 t CO_2-eq t^{-1}), indicating major potential for GHG mitigation when secondary (recycled) aluminum and low-carbon electricity are used.

However, several caveats must be considered for upscaling:

- *Slag volumes:* The SMR observed in this study was 1.34 kg/kg and 1.79 kg/kg for the Nchwaning pre-reduced ores in a retort furnace and plasma furnace, respectively. For the UMK ore pre-reduced in the retort furnace, the SMR was observed to be 1.87 kg/kg.
- *Emission normalization and abatement:* Pilot stack concentrations indicate low gaseous emissions by concentration, but normalized emissions (kg t^{-1}) are sensitive to assumed flue volumes and capture efficiency. Industrial implementations would need robust abatement and continuous monitoring to ensure compliance and low net emissions after normalization.
- *Operational stability:* Measured current/voltage/power deviations (mean deviations $\sim$10–12%) show room for process control improvements; stability gains typically reduce electrode/refractory wear and raise delivered power, improving SEC further at scale.

Overall, the pilot campaign results indicate that the HAlMan process can deliver major energy and emission advantages versus conventional carbothermic HCFeMn production,

while presenting specific challenges (notably slag volumes and process stability) that must be targeted in scale-up and integration studies.

5. Conclusions

This investigation involved examining the smelting–aluminothermic reduction of hydrogen pre-reduced manganese ores within a 200 kW DC arc furnace with an interest in the effects of properties of pre-reduced UMK and Nchwaning manganese ores and the effect of two pre-reduction approaches, namely, the vertical retort-packed bed furnace and the rotary plasma furnace. The scope integrated technical, material, environmental, and operational sustainability metrics to establish the viability of the novel HAlMan process route. This investigation successfully validated the HAlMan process route on a 200 kW DC arc furnace pilot scale. By evaluating technical, material, and environmental metrics across different ore types and pre-reduction methods (vertical retort vs. rotary plasma), this study establishes a robust foundation for low-carbon ferroalloy production. This study successfully established a novel, multi-stage validation of the HAlMan process route, integrating hydrogen pre-reduction with smelting–aluminothermic reduction of manganese ores on a 200 kW DC arc furnace pilot scale. The investigation presented how the extent of pre-reduction for both UMK and Nchwaning ores directly influenced subsequent smelting performance.

From a partial process estimate energy perspective, stable furnace operation was consistently achieved across all experimental campaigns, with load factors regularly reaching 96.89%, demonstrating efficient furnace utilization. Despite arc instability observed at higher voltages (100 V), necessitating voltage adjustments in specific trials, the DC arc furnace exhibited robust adaptability to variations in feed composition, specific energy requirement setpoints, and flux/reductant additions. The SER was effectively maintained within the targeted range of 0.80–1.15 kWh/kg, and thermal efficiency calculations underscored the significant energetic contribution of exothermic aluminothermic reactions. The strong correlation between average power and feed rate further validated the reliability of the applied energy balance methodology at this pilot scale.

Material efficiency indicators confirmed satisfactory system performance. Overall elemental accountability consistently exceeded 95% for all major elements, indicating robust mass balance closure. High iron recovery (approximately 96%) to the metallic phase was observed, while manganese recovery reached about 66%, with the remainder predominantly partitioning to the slag. Silicon exhibited moderate recovery, whereas aluminum primarily reported to the slag, aligning with its role as the primary reductant. Reductant efficiencies varied between approximately 19% and 75%, influenced by ore characteristics and pre-reduction approach, thus emphasizing the critical roles of pre-reduction extent and slag chemistry in optimizing aluminum utilization.

The slag-to-metal ratio varied from 1.34 to 1.87 kg/kg. Nchwaning ore generally produced lower SMRs compared to UMK ore, signifying improved material efficiency and reduced slag generation. Comparing pre-reduction approaches, the vertical retort route demonstrated a lower SMR (1.34 kg/kg) and reduced refractory consumption rate (0.1051 kg MgO/kg metal) than the rotary plasma route. These findings suggest notable advantages for downstream smelting performance and furnace lining longevity. Refractory consumption rates, ranging from 0.1051 to 0.1838 kg MgO/kg metal, reflected the interplay of slag chemistry and thermal conditions. Electrode consumption also varied significantly.

An environmental assessment, conducted according to ISO 14040 and ISO 14044 attributional LCA principles, confirmed low measured stack emissions. Average particulate matter (3.5 mg/Nm^3), negligible SO_2, and low NO_x concentrations demonstrate that this integrated hydrogen pre-reduction and smelting–aluminothermic reduction route can op-

erate within stringent regulatory frameworks. The minimal direct CO_2 emissions from the furnace, coupled with the potential for low-carbon hydrogen and renewable electricity, position this process as a highly promising pathway toward decarbonized manganese alloy production.

The integration of hydrogen pre-reduction with smelting–aluminothermic reduction in a DC arc furnace offers a technically robust and environmentally advantageous alternative to conventional carbothermic submerged arc furnace routes. The vertical retort pre-reduction approach demonstrated superior overall smelting performance concerning slag generation, refractory wear, and electrode consumption, while both approaches ensured high furnace utilization and stable operation. These findings affirm that hydrogen-assisted pre-reduction combined with smelting–aluminothermic reduction significantly enhances manganese recovery, reduces carbon intensity, and improves operational sustainability. Future research should prioritize optimizing pre-reduction extent, refining aluminum dosing strategies, enhancing manganese recovery from slag, and conducting detailed techno-economic analyses at an industrial scale to fully establish the commercial viability of this low-carbon manganese production pathway.

Supplementary Materials: The following supporting information can be downloaded at: https://www.mdpi.com/article/10.3390/met16070794/s1, Table S1: UMK QXRD mineral phases, stoichiometric total removable oxygen per mineral phase and the total removable oxygen; Table S2: Nchwaning ore QXRD mineral phases, stoichiometric total removable oxygen per mineral phase and the total removable oxygen.

Author Contributions: D.M.: Conceptualization, Methodology, Campaign Execution, Data curation, Writing—original draft, review and editing; S.T.: Conceptualization, Methodology, Formal analysis, Technical supervision, Writing—review; M.M.: Conceptualization, Methodology, Campaign Execution, Formal analysis, Writing—review; J.S.: Conceptualization, Methodology, Data curation, Writing, Review and editing; E.M.: Conceptualization, Methodology, Formal analysis, Technical supervision, Writing—review. All authors have read and agreed to the published version of the manuscript.

Funding: This study was financially supported by the European Union's Horizon Europe program HAlMan project under the grant number 101091936.

Data Availability Statement: Raw research data will be made available upon formal request.

Acknowledgments: The authors wish to acknowledge SINTEF for supplying the Nchwaning manganese ore pre-reduced in a rotary plasma furnace, which was essential for the comparative scope of this study. The authors further extend sincere and deep appreciation to Mintek for support through technical acumen and operational diligence. We remain indebted to all HAlMan consortium partners for their valuable discussions and insights, which contributed to the interpretation and contextualization of the results.

Conflicts of Interest: The authors declare no conflicts of interest.

References

1. Han, Y.; Li, C.; Wang, H. Primary Study on Medium and Low Carbon Ferromanganese Production by Blowing CO_2-O_2 Mixtures in Converter. *Metals* **2022**, *12*, 682. [CrossRef]
2. Davies, J.; Tangstad, M.; Schanche, T.L.; du Preez, S.P. Pre-reduction of United Manganese of Kalahari Ore in CO/CO_2, H_2/H_2O, and H_2 Atmospheres. *Metall. Mater. Trans. B* **2023**, *54*, 515–535. [CrossRef]
3. Kudyba, A.; Akhtar, S.; Johansen, I.; Safarian, J. Aluminothermic reduction of manganese oxide from selected MnO-containing slags. *Materials* **2021**, *14*, 356. [CrossRef] [PubMed]
4. Mukono, T.; Reiersen, H.S.; Schanche, T.L.; Wallin, M.; Tangstad, M. Prereduction Behavior of Manganese Ores with Solid Carbon and in CO/CO_2 Gas Atmosphere. *Metall. Mater. Trans. B* **2022**, *53*, 3292–3305. [CrossRef]
5. Mukono, T.; Wallin, M.; Tangstad, M. Phase Distribution During Slag Formation in Mn Ferroalloy Production. *Metall. Mater. Trans. B* **2022**, *53*, 1122–1135. [CrossRef]

6. Sarkar, A.; Schanche, T.L.; Wallin, M.; Safarian, J. Evaluating the Reaction Kinetics on the H2 Reduction of a Manganese Ore at Elevated Temperatures. *J. Sustain. Metall.* **2024**, *10*, 2085–2103. [CrossRef]
7. Surup, G.R.; Trubetskaya, A.; Tangstad, M. Life Cycle Assessment of Renewable Reductants in the Ferromanganese Alloy Production: A Review. *Processes* **2021**, *9*, 185. [CrossRef]
8. Harvey, J.-P.; Courchesne, W.; Vo, M.D.; Oishi, K.; Robelin, C.; Mahue, U.; Leclerc, P.; Al-Haiek, A. Greener reactants, renewable energies and environmental impact mitigation strategies in pyrometallurgical processes: A review. *MRS Energy Sustain.* **2022**, *9*, 212–247. [CrossRef] [PubMed]
9. Bajpai, A.; Ratzker, B.; Shankar, S.; Raabe, D.; Ma, Y. Sustainable Pre-reduction of Ferromanganese Oxides with Hydrogen: Heating Rate-Dependent Reduction Pathways and Microstructure Evolution. *arXiv* **2025**, arXiv:2507.10451. [CrossRef]
10. Al-Nasser, M.; Kharicha, A.; Barati, H.; Pichler, C.; Hackl, G.; Gruber, M.; Ishmurzin, A.; Redl, C.; Wu, M.; Ludwig, A. Toward a Simplified Arc Impingement Model in a Direct-Current Electric Arc Furnace. *Metals* **2021**, *11*, 1482. [CrossRef]
11. HAlMan EU Project. Sustainable Hydrogen and Aluminothermic Reduction Process for Manganese. Available online: https://halman-project.eu/ (accessed on 14 April 2026).
12. Safarian, J. The Production of Manganese and Its Alloys Through the HAlMan Process. In *The Minerals, Metals & Materials Series*; Springer: Cham, Switzerland, 2023; pp. 749–756. [CrossRef]
13. Sarkar, A.; Schanche, T.L.; Wallin, M.; Safarian, J. Kinetics Study on the H_2 Reduction of Nchwaning Manganese Ore at Elevated Temperatures. *Int. J. Miner. Metall. Mater.* **2025**, *32*, 1091–1102. [CrossRef]
14. Sarkar, A.; Tang, K.; Safarian, J. Hydrogen Reduction Kinetics of a High-Carbonate Manganese Ore in Raw and Calcined Forms under Isothermal Conditions. *Int. J. Hydrogen Energy* **2026**, *200*, 152919. [CrossRef]
15. *ASTM E1019*; Standard Test Methods for Determination of Carbon, Sulfur, Nitrogen, and Oxygen in Steel, Iron, Nickel, and Cobalt Alloys by Various Combustion and Inert Gas Fusion Techniques. ASTM International: West Conshohocken, PA, USA, 2024.
16. Schanche, T.L.; Tangstad, M. Isothermal reduction of Nchwaning manganese ore in $CO/CO_2/H_2$ atmospheres. In Proceedings of the 16th International Ferro-Alloys Congress (INFACON XVI) 2021, Trondheim, Norway, 27–29 September 2021. [CrossRef]
17. Sun, H.; Adetoro, A.A.; Wang, Z.; Pan, F.; Li, L. Direct Reduction Behaviors of Titanomagnetite Ore by Carbon Monoxide in Fluidized Bed. *ISIJ Int.* **2016**, *56*, 936–943. [CrossRef]
18. Zheng, H.; Daghagheleh, O.; Wolfinger, T.; Taferner, B.; Schenk, J.; Xu, R.S. Fluidization behavior and reduction kinetics of pre-oxidized magnetite-based iron ore in a hydrogen-induced fluidized bed. *Int. J. Miner. Metall. Mater.* **2022**, *29*, 1873–1881. [CrossRef]
19. Ngoy, D.M.B.; Sukhomlinov, D.; Tangstad, M. Pre-reduction Behaviour of Manganese Ores in H_2 and CO Containing Gases. *ISIJ Int.* **2020**, *60*, 2326–2334. [CrossRef]
20. Moskal, M.; Migas, P.; Karbowniczek, M. Multi-Parameter Characteristics of Electric Arc Furnace Melting. *Materials* **2022**, *15*, 1601. [CrossRef] [PubMed]
21. Logar, V.; Škrjanc, I. The Influence of Electric-Arc-Furnace Input Feeds on its Electrical Energy Consumption. *J. Sustain. Metall.* **2021**, *7*, 1013–1026. [CrossRef]
22. Hernández, J.D.; Onofri, L.; Engell, S. Modeling and Energy Efficiency Analysis of the Steelmaking Process in an Electric Arc Furnace. *Metall. Mater. Trans. B* **2022**, *53*, 3413–3441. [CrossRef]
23. Safarian, J. Effect of Calcination of Manganese Ore on Reducing Hydrogen and Energy Consumptions in Hydrogen-Based Direct Reduction Process. *Metals* **2026**, *16*, 117. [CrossRef]
24. Bertuccioli, L.; Chan, A.; Hart, D.; Lehner, F.; Madden, B.; Standen, E. *Study on Development of Water Electrolysis in the EU*; Fuel Cells and Hydrogen Joint Undertaking (FCH JU): Brussels, Belgium, 2014.
25. Wanjari, A. Methods to optimize energy consumption in Conarc furnaces. *SN Appl. Sci.* **2021**, *3*, 873. [CrossRef]
26. Baba, A.A.; Ibrahim, L.; Adekola, F.A.; Bale, R.B.; Ghosh, M.K.; Sheik, A.R.; Pradhan, S.R.; Ayanda, O.S.; Folorunsho, I.O. Hydrometallurgical Processing of Manganese Ores: A Review. *J. Miner. Mater. Charact. Eng.* **2014**, *2*, 31–47.
27. Mukono, T.; Gjøvik, J.E.; Gärtner, H.; Wallin, M.; Ringdalen, E.; Tangstad, M. Extent of ore prereduction in pilot-scale production of high carbon ferromanganese. In Proceedings of the 16th International Ferro-Alloys Congress (INFACON XVI) 2021, Trondheim, Norway, 27–29 September 2021. [CrossRef]
28. Coetsee, T. MnO reduction in high carbon ferromanganese production: Practice and theory. *J. S. Afr. Inst. Min. Metall.* **2018**, *118*, 1145–1156.
29. Tangstad, M.; Bublik, S.; Haghdani, S.; Einarsrud, K.E.; Tang, K. Slag Properties in the Primary Production Process of Mn-Ferroalloys. *Metall. Mater. Trans. B* **2021**, *52*, 3688–3707. [CrossRef]
30. Safarian, J.; Kolstad, H.; Tangstad, M. A sustainable process to produce manganese and its alloys. *Processes* **2025**, *10*, 27. [CrossRef]
31. Finnholm, T.; Klemettinen, L.; Tammela, J.; Taskinen, P.; O'Brien, H.; Michallik, R.M.; Lindberg, D. Deportment of Minor Elements in Industrial Copper Smelting. *JOM* **2025**, *77*, 3970–3984. [CrossRef]

32. Pankka, I.; Salminen, J.; Taskinen, P.; Lindberg, D. Thermodynamic Modeling of Elemental Distributions of Trace Elements in Non-ferrous Iron Residue Hydrogen Reduction. *JOM* **2023**, *75*, 2026–2033. [CrossRef]
33. Steenkamp, J.D.; Banda, K.W.; Bezuidenhout, P.J.A.; Denton, G.M. New Laboratory and Pilot Techniques Applied at Mintek in Aid of Furnace Containment System Designs. *JOM* **2021**, *74*, 203–212. [CrossRef]
34. Timoshenko, S.; Gubinski, M.; Niemtsev, E. Energy-efficient solutions of foundry class steelmaking electric arc furnace. *Nauk. Visnyk Natsionalnoho Hirnychoho Universytetu* **2021**, *3*, 81–87. [CrossRef]
35. *ISO 14040:2006*; Environmental Management—Life Cycle Assessment—Principles and Framework. International Organization for Standardization: Geneva, Switzerland, 2006.
36. *ISO 14044:2006/Amd 1:2017/Amd 2:2020*; Environmental Management—Life Cycle Assessment—Requirements and Guidelines. International Organization for Standardization: Geneva, Switzerland, 2020.
37. Windsor, R.; Cinelli, M.; Coles, S.R. Comparison of tools for the sustainability assessment of nanomaterials. *Curr. Opin. Green Sustain. Chem.* **2018**, *12*, 69–75. [CrossRef]
38. *ISO/IEC 17025:2017*; General Requirements for the Competence of Testing and Calibration Laboratories. International Organization for Standardization: Geneva, Switzerland; International Electrotechnical Commission: Geneva, Switzerland, 2017.
39. Mokgosi, M.; Faulds, B.; Dube, J. STACK Emissions Monitoring Report 2025, July 2025. Available online: https://teams.public.onecdn.static.microsoft/evergreen-assets/safelinks/2/atp-safelinks.html (accessed on 22 July 2025).
40. Ernst, M.; Tangstad, M.; du Preez, S.P. Pre-reduction of Nchwaning manganese ore in CO/CO_2, H_2/H_2O, and H_2 atmospheres. *Miner. Eng.* **2024**, *216*, 108854. [CrossRef]
41. Perroy, É.; Lucas, D.; Debusschere, V. Provision of Frequency Containment Reserve Through Large Industrial End-Users Pooling. *IEEE Trans. Smart Grid* **2019**, *11*, 26–36. [CrossRef]
42. Kleimt, B.; Krieger, W.; Vasallo, D.M.; Ayarza, A.A.; Unamuno, I. Model-Based Decision Support System for Electric Arc Furnace (EAF) Online Monitoring and Control. *Metals* **2023**, *13*, 1332. [CrossRef]
43. Mauer, G. Multiple Electrodes and Cascaded Nozzles: A Review of the Evolution of Modern Plasma Spray Torches. *J. Therm. Spray Technol.* **2024**, *33*, 2135–2149. [CrossRef]
44. Jones, R.T.; Reynolds, Q.G.; Alport, M.J. DC arc photography and modelling. *Miner. Eng.* **2002**, *15*, 985–991. [CrossRef]
45. Mironov, Y.M. Effect of arcing on the electrical parameters and the technical-and-economic indices of an arc furnace. *Russ. Metall.* **2019**, *2019*, 1238–1244. [CrossRef]
46. Paranchuk, Y.; Lis, M. Double-circuit adaptive system of fuzzy phase-autonomous and energy-efficient control of arc furnace electric modes. *Energies* **2023**, *16*, 5350. [CrossRef]
47. Bergman, K.; Kjellberg, B. DC arc furnace technology applied to smelting applications. In Proceedings of the Ninth International Ferroalloys Congress, Quebec City, QC, Canada, 3–6 June 2001; pp. 80–89.
48. Guerra-Serrano, J.; Sánchez Roca, Á.; González-Yero, G.; Sánchez Orozco, M.C.; Pérez, M.; Jiménez Macías, E.; Blanco-Fernández, J. New arc stability index for industrial AC three-phase electric arc furnaces based on acoustic signals. *Sensors* **2020**, *20*, 6840. [CrossRef] [PubMed]
49. Trembach, B.; Silchenko, Y.; Sukov, M.; Sadovyi, K.; Knyazev, S.A.; Krbata, M.; Balenko, O.; Kniazieva, H.; Kabatskyi, O. Investigation of the arc stability during self-shielded flux-coated arc welding with exothermic additions. *Res. Sq.* **2023**. [CrossRef] [PubMed]
50. Blažič, A.; Škrjanc, I.; Logar, V. Arc Quality Index Based on Three-Phase Cassie–Mayr Electric Arc Model of Electric Arc Furnace. *Metals* **2024**, *14*, 338. [CrossRef]
51. Narzullayev, B.; Eshmirzaev, M.A. Causes of the appearance of current waves in high voltage electric arc furnaces, and methods of their reduction. *E3S Web Conf.* **2023**, *417*, 3003. [CrossRef]
52. Fleuriault, C.; Grogan, J.; White, J. Electric arc smelting: Fleuriault, Grogan, and White. *JOM* **2019**, *71*, 321–322.
53. Xi, X.; Li, S.; Li, C.; Pan, H.; Wang, J.; Zhu, R. Research on technical parameters of electrical arc furnace steelmaking based on direct reduced iron as raw material. *Ironmak. Steelmak. Process. Prod. Appl.* **2024**, *51*, 947. [CrossRef]
54. Gregurek, D.; Peng, Z.; Wenzl, C.; White, J.F. Fe alloys: Production and metallurgical aspects: Part II. *JOM* **2016**, *69*, 323–324. [CrossRef]
55. Randhawa, N.S.; Minj, R.K.; Kumar, K. Eco-friendly low-carbon manganese ferroalloy production for cleaner steel technologies. *Clean. Eng. Technol.* **2024**, *21*, 100784. [CrossRef]
56. Hockaday, L.; Dinter, F.; Reynolds, Q.G. The thermal decomposition kinetics of carbonaceous and ferruginous manganese ores in atmospheric conditions. *J. S. Afr. Inst. Min. Metall.* **2023**, *123*, 391–398. [CrossRef] [PubMed]
57. Kumar, P.; Safarian, J. Effect of pre-reduction of manganese ore by hydrogen on its smelting behavior and interaction with stable oxides. *J. Sustain. Metall.* **2025**, *11*, 2980–3000. [CrossRef]
58. Kar, M.K.; Safarian, J. Studying the alkaline leachability of calcium aluminate slag produced from aluminothermic reduction of a hydrogen reduced manganese ore. *Sep. Purif. Technol.* **2025**, *382*, 135878. [CrossRef]

59. Boldrini, A.; Koolen, D.; Crijns-Graus, W.; Worrell, E.; van den Broek, M. Flexibility options in a decarbonising iron and steel industry. *Renew. Sustain. Energy Rev.* **2023**, *189*, 113988. [CrossRef]
60. Rimal, V.; Tangstad, M. Kinetics of manganese reduction comparing synthetic slags and ores for ferromanganese production. *Metall. Mater. Trans. B* **2025**, *56*, 2731–2747. [CrossRef]
61. Lee, Y.E.; Kolbeinsen, L. Behavior of Slag in Ferromanganese and Silicomanganese Smelting Process. *Metall. Mater. Trans. B* **2021**, *52*, 2931–2945. [CrossRef]
62. Li, R.; Liu, L.; Zhang, L.; Sun, J.; Shi, Y.; Yu, B. Effect of squeeze casting on microstructure and mechanical properties of hypereutectic Al–xSi alloys. *J. Mater. Sci. Technol.* **2017**, *33*, 404–410. [CrossRef]
63. Kumar, P.; Safarian, J. Aluminothermic Reduction of HCFeMn Slag and Hydrogen Based Pre-reduced Mn Ore. In *HAlMan Bi-Annual Meeting WP 3-Task 3.2 Progress Report*; unpublished; Department of Materials Science and Engineering, Norwegian University of Science and Technology (NTNU): Trondheim, Norway, 2024.
64. Ahmed, A.; Halfa, H.; El-Fawakhry, M.K.; El-Faramawy, H.; Eissa, M. Parameters Affecting Energy Consumption for Producing High Carbon Ferromanganese in a Closed Submerged Arc Furnace. *J. Iron Steel Res. Int.* **2014**, *21*, 666–672. [CrossRef]
65. Vasebi, A.; Poulin, É.; Hodouin, D. Selecting proper uncertainty model for steady-state data reconciliation—Application to mineral and metal processing industries. *Miner. Eng.* **2014**, *65*, 130–144. [CrossRef]
66. Bascur, O.A.; Linares, R. Solving Metal Losses Problems: Metallurgical Mass Balances. *IFAC Proc. Vol.* **2004**, *37*, 143–148. [CrossRef]
67. Teixeira, P.; Lopes, H.; Gulyurtlu, I.; Lapa, N. Uncertainty estimation to evaluate mass balances on a combustion system. *Accred. Qual. Assur.* **2012**, *17*, 159–166. [CrossRef]
68. Subasinghe, G.K.N.S. A transparent technique for mass balancing and data adjustment of complex metallurgical circuits. *Miner. Process. Extr. Met. Trans. I.M.M. Sect. C* **2009**, *118*, 162–167. [CrossRef]
69. Arzpeyma, N.; Alam, M.; Gyllenram, R.; Jönsson, P.G. Model Development to Study Uncertainties in Electric Arc Furnace Plants to Improve Their Economic and Environmental Performance. *Metals* **2021**, *11*, 892. [CrossRef]
70. Kudyba, A.; Safarian, J. Manganese and Aluminium Recovery from Ferromanganese Slag and Al White Dross by a High Temperature Smelting-Reduction Process. *Materials* **2022**, *15*, 405. [CrossRef] [PubMed]
71. Ma, Y.; Moosavi-Khoonsari, E.; Kero, I.; Tranell, G. Element Distribution in the Silicomanganese Production Process. *Metall. Mater. Trans. B* **2018**, *49*, 2444–2457. [CrossRef]
72. Eissa, M.; El-Faramawy, H.; Farid, G. Production of high carbon ferromanganese using manganese rich slag in the charge. *Steel Res.* **1998**, *69*, 373–380. [CrossRef]
73. Eissa, M.; El-Faramawy, H.; Ahmed, A.; Nabil, S.; Halfa, H. Parameters Affecting the Production of High Carbon Ferromanganese in Closed Submerged Arc Furnace. *J. Miner. Mater. Charact. Eng.* **2012**, *11*, 1–20. [CrossRef]
74. Wei, W.; Samuelsson, P.; Jönsson, P.G.; Gyllenram, R.; Glaser, B. Energy Consumption and Greenhouse Gas Emissions of High-Carbon Ferrochrome Production. *JOM* **2023**, *75*, 1206–1220. [CrossRef]
75. Edwards, L.; Hunt, M.; Weyell, P.; Nord, J.A.; Côté, J.; Coulombe, P.; Morais, N. Quantifying the Carbon Footprint of the Alouette Primary Aluminum Smelter. *JOM* **2022**, *74*, 4909–4919. [CrossRef]
76. Acheampong, T.; Tyce, M. Navigating the energy transition and industrial decarbonisation: Ghana's latest bid to develop an integrated bauxite-to-aluminum industry. *Energy Res. Soc. Sci.* **2023**, *107*, 103337. [CrossRef]
77. Leme, R.D.; Nunes, A.O.; Costa, L.B.M.; Silva, D.A.L. Creating value with less impact: Lean, green and eco-efficiency in a metalworking industry towards a cleaner production. *J. Clean. Prod.* **2018**, *196*, 517–534. [CrossRef]
78. Van Berkel, R. Eco-efficiency in the Australian minerals processing sector. *J. Clean. Prod.* **2006**, *15*, 772–781. [CrossRef]
79. Spooner, M.P. *Methods and Tools for the Statistical Data Analysis of Large Datasets Collected from Bio-Based Manufacturing Processes*; Technical University of Denmark: Lyngby, Denmark, 2018; p. 152. Available online: https://local.forskningsportal.dk/local/dki-cgi/ws/cris-link?src=dtu&id=dtu-c044b23c-a1c1-4a9c-a2cd-bac25ea815a4&ti=Methods%20and%20tools%20for%20the%20statistical%20data%20analysis%20of%20large%20datasets%20collected%20from%20bio-based%20manufacturing%20processes (accessed on 15 February 2026).
80. Yang, Y.; Loxton, R.; Rohl, A.L.; Bùi, H.T. Long-term maintenance optimization for integrated mining operations. *Optim. Eng.* **2023**, *25*, 1817–1848. [CrossRef]
81. Kero, I.; Eidem, P.A.; Ma, Y.; Indresand, H.; Aarhaug, T.A.; Grådahl, S. Airborne Emissions from Mn Ferroalloy Production. *JOM* **2018**, *71*, 349–365. [CrossRef]

Disclaimer/Publisher's Note: The statements, opinions and data contained in all publications are solely those of the individual author(s) and contributor(s) and not of MDPI and/or the editor(s). MDPI and/or the editor(s) disclaim responsibility for any injury to people or property resulting from any ideas, methods, instructions or products referred to in the content.